

PLUME-MoM 1.0: A new integral model of  
volcanic plumes based on the method of moments

M. de' Michieli Vitturi, A. Neri and S. Barsotti

July 24, 2015

## Responses to Referee 1

**R1.** *Title and pg 3746 ln 2: The description of the model as 1-D is misleading. The model gives three-dimensional results (the wind can change direction and, with a model for the radial variation of the fields, the three dimensional character of the plume can be reconstructed). Rather, the model has only 1 independent variable, the arc-length along the centreline. It would be better to describe the model as an integral model, as it is derived by integrating the point-wise conservation equations over the plume cross-section.*

**A.** We agree with the suggestion of the referee. We removed 1D from the title and the text and the model is now described as an integral model.

**R1.** *Pg 3749: How are the moments defined in equation (1) related to other descriptions of the shape of the distribution such as the mean, variance, skewness, kurtosis? Could central and standardized moments be used to make this connection between descriptions of the distributions?*

**A.** The central moments can be expressed as terms of the raw moments (i.e., those taken about zero) using a binomial transform. In this way it is also possible to relate the moments of the distribution with the mean, variance, skewness, kurtosis. We added a sentence to clarify this fact in the manuscript at the end of section 2.1.

**R1.** *Pg 3749 ln 17: Does the prefactor in  $M(3)$  assume spherical particles? Can the same interpretations of the moments be made if the particles are not spherical, as is typical for volcanic pyroclasts? I recommend writing  $/6M(3)j = s,j$  as  $s,j$  is used subsequently.*

**A.** The referee is correct: the prefactor assumes spherical particles and this is now clarified in the text. For particles with different shapes, if volume scales with the third power of length, we can relate the particle volume  $V$  and particle length  $L$  through a volumetric shape factor  $k_v$ :  $V=k_v L^3$ . It is possible to introduce a sphericity parameter to relate the diameter with the particle volume.

**R1.** *Pg 3752 equation (7): The quantities  $k_1$ ,  $k_2$ ,  $k_3$  are not defined and their values are not given. Dimensional analysis shows that their dimensions differ do these quantities have a physical meaning? Also,  $C D$  should be defined and the used value given.*

**A.** The values of the different parameters have been added to the text.

**R1.** *Pg 3753 equation (10): It appears that there has been an implicit definition the square bracket notation as*

$$[g(D)]^{(i)} = \frac{1}{M_j^{(i)}} \int_0^\infty g(D) f_j(D) D^i dD.$$

*It would useful to make this definition explicit, as it is used subsequently. Also, as the denominator in equation (10) doesn't depend on  $D$  it can be taken out of the integral.*

**A.** The definition of the moments of other variables is at page 3750, Eq. 2 (of the original manuscript). The square brackets are used in Eq. 10 (of the

original manuscript) because the moment appearing on the right-hand side is not the moment of a single variable but the moments of the product of two variables. The denominator has been taken out of the integral.

**R1.** Pg 3754: the use of two variants of the phi symbol ( $\phi$  and  $\varphi$ ) (one used for the phi-scale size and the other for the particle mass fraction distribution) is not a very convenient notation.

**A.** The variable  $\gamma$  is now used for the particle mass fraction distribution.

**R1.** Pg 3754: it should be explicitly stated that  $\Pi_j^{(0)} = x_{s,j}$ .

**A.** It is stated in the text that the moment  $\Pi_j^{(0)}$  is the mass fraction of the  $j$ -th solid phase  $x_{s,j}$  with respect to the gas-particles mixture

**R1.** Pg 3754 equation (13): there is another use of the square bracket notation, but this is inconsistent with the previous use (see comment 5). In particular, the kernel and variable of integration differ in these definitions. A new notation is needed.

**A.** As stated before, the square bracket are not used for any particular notation. The notation used here is only the superscript (0) for the moment of the heat capacity. In any case, the square bracket is superfluous in Eq. 13 (of the original manuscript) and also the denominator in the right-hand side should be removed, as well as the denominator in the right-hand side of Eq. 14 (of the original manuscript).

**R1.** Pg 3755 ln 5:  $\phi$  is used to denote an angle, but it has previously been used to denote the particle size.  $x$  has also been used previously.

**A.** A different notation has been introduced for the angle, while we do not think that there are problems with the similar notations used for the horizontal coordinate  $x$  and the mass fraction  $x_{s,j}$ .

**R1.** Section 3: There are numerous assumptions implicit in the equations presented. These assumptions must be made explicit.

**A.** The assumptions have been made explicit in the text adding the following lines: "The model assumes an homogeneous mixture of particles and gases with thermal and mechanical equilibrium between all phases. Aggregation and breakage effects are not considered here and consequently density does not change with time. Finally, the model does not consider effects of humidity and water phase changes."

**R1.** The symbol  $\alpha$  has already been used.

**A.** A subscript has been added to the symbols used for the two entrainment coefficients.

**R1.** The entrainment formulation given in equation (20) was first proposed by Hewett et al 1971 ([http://dx.doi.org/10.1016/0004-6981\(71\)90028-X](http://dx.doi.org/10.1016/0004-6981(71)90028-X)). This reference should be used.

**A.** The suggested reference has been added.

**R1.** Pg 3737 ln 19: The text states that the equations for the conservation of momentum (equations 22 and 23) can be derived from the conservation of mass (equation 21). This is not correct independent information is required (Newtons second law). This also applies to the similar discussion on pg 3761.

**A.** The text has been corrected and now it states: From Newton’s second law and the variation of mass flux ....

**R1.** Pg 3758 ln 18: *The bulk densities  $\rho_{atm}^B$  and  $\rho_{wv}^B$  are not defined. Need to state how  $\rho_g$  is determined from the bulk densities.*

**A.** The definitions of the bulk densities have been added to the text: "bulk density of the particles of the  $j$ -th family (i.e. the mass of particles of the  $j$ -th family per unit volume of gas-particles mixture)".

**R1.** Pg 3759: *The derivation of the rate of change of the mixture specific heat capacity is not clear. Why are partial derivatives used (what variables are held fixed)? Why is the second term on the right-hand-side written in this way?*

Pg 3760 lns 7-10: *Does the use of  $\rho_{mix}$  and  $C_{mix}$  at  $s$  to find  $T$  at  $s+ds$  result in a first-order scheme? I suggest removing these lines as the direct integration of equations (28) and (30) are preferred?*

**A.** The partial derivatives have been changed to total derivatives. Eqs. 28 and 30 have been added to close the system of equations and to avoid, as stated in the text, the use of  $\rho_{mix}$  and  $C_{mix}$  at  $s$  when calculating the updated variables at  $s + ds$ . Without the new value of  $C_{mix}$ , given by Eq. 30, it is not possible to find the value of  $T$  at  $s + ds$  from the solution of Eq. 24 only. In the same way, the updated value of the gas constant is needed to compute the new density at  $s + ds$ . In any case, the text has been rewritten to clarify this fact.

**R1.** Section 4.1: *There is extensive use of jargon in the description of this algorithm that results in a lack of clarity. In particular:*

(i) *the term realizable moment set should be avoided or defined.*

(ii) *the term invalid moment set requires clarification.*

(iii) *what is moment corruption and how can it be diagnosed?*

(iv) *Hankel-Hadamard determinants require definition or reference.*

(v) *why do nodes within the support of the distribution and positive weights guarantee accuracy of the algorithm? An explanation and reference are required.*

(vi) *it not clear at which point in the predictor-corrector numerical integration the algorithm is used. Is it in both the predictor and corrector step?*

**A.** (i) the definition of realizable moment set is given at lines 20-21: meaning that there exists a particle size distribution resulting in that specific set of moments. In any case, we moved it after the first use of the term realizable to make it clearer.

(ii) the sentence has been removed.

(iii) the following text has been added: "the problem of moment corruption (i.e. the transformation during the integration of the moment-transport equations of a realizable set of moments into an unrealizable one)"

(iv) a reference to Gautschi, 2004 has been added

(v) a reference has been added.

(vi) the algorithm is used in both the predictor and corrector step. This has been clarified in the text.

**R1.** Pg 3765 ln 1: *The initial moments are evaluated analytically... This can only be true if a probability model is provided for the initial particle distribution and the model is sufficiently integrable to calculate the required moments.*

**A.** The sentence has been changed stating that the moments are evaluated analytically for the initial particle distribution presented in this work. We remark here that the distributions considered in the paper are not probability densities and the integral over the size spectrum can be different from 1.

**R1.** *Pg 3765 lns 4-8: This paragraph is not clear. I'd recommend re-writing, perhaps including the equation for  $\varphi(\phi)$  given in equation (53) moved to this point.*

**A.** Equation 53 has been moved as suggested by the referee.

**R1.** *Pg 3768: The justification for using the formulation based on the moments of mass fraction distribution rather than the number distribution (i.e. that the first three moments can be combined to give the mean and variance of a normal distribution) seems weak. Surely it is natural to use the moments of the particle mass fraction distribution to track changes in quantities derived from and describing the mass fraction distribution.*

**A.** It seems to us that what is written in the text is exactly what the referee says, i.e. that it is natural to use the moments of the particle mass fraction distribution to track changes in quantities derived from and describing the mass fraction distribution:

”when we want to track the changes of the mass fraction averaged diameter and its SD (or variance) in the  $\phi$  scale during the plume rise, it is preferred to use a formulation based on the moments  $\Pi^{(i)}$ ”.

We also remark that the first three moments can be combined to give the mean and variance of any distribution, not only of a normal distribution.

**R1.** *Section 5.3: It should be noted that the sensitivity analysis performed is only a partial sensitivity analysis. Only a small subset of the model parameters and inputs are varied. The sensitivity results are therefore conditional on the values taken for the fixed parameters. In particular, it is possible that different inferences might be made if some of the fixed parameters take different values. gPCE: The generalized Polynomial Chaos Expansion is more similar to a spectral method rather than a finite element method, as the expansion is a high order polynomial posed on the whole domain of the input variable rather than a series of low-order polynomials each posed on a collection of subset (elements) covering the input domain. The multidimensional integral referred to on pg 3773 should be given or references provided - as written it is not clear how to determine the expansion coefficients, and there are several methods for doing this. A reference is needed for Clenshaw-Curtis quadrature. It should also be noted that the requirement to evaluate multidimensional integrals might result in a high computational cost when there are a large number of inputs and when the integrand is not well behaved.*

*Pg 3774: When comparing the LHS and gPCE approaches, there is a choice of using 1000 and 2000 samples for the LHS. It would be useful to show small sample sizes for the LHS, to give a suitable lower bound on the number of samples. In particular, as the response surfaces found here are very smooth and with small variation, it is possible the smaller LHS would give good results here.*

**A.** We agree with the referee that we are not presenting a full sensitivity analysis, but this is out of the scope of the paper. In the manuscript we want

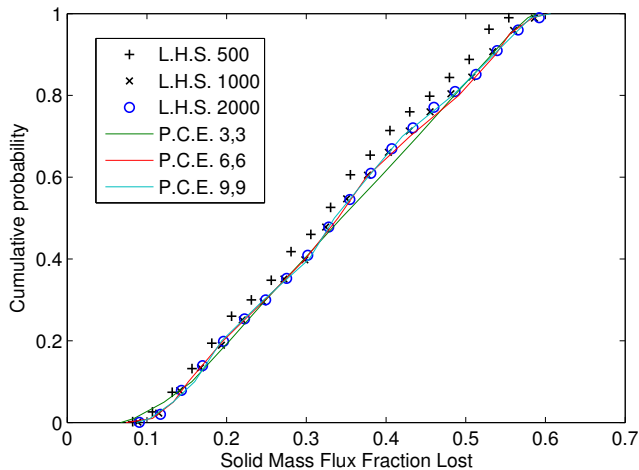


Figure 1: Cumulative distributions and response surfaces for test Case 1 (weak plume without wind).

to present a plume model based on the method of moments, and one of the main advantages of the method is the capability to track in an effective way the changes of the mean and standard deviation of the particle distribution (with 4 moments only with the formulation based on the mass fraction). For this reason we presented a sensitivity analysis based on the uncertainty on these two parameters described by the moments.

Regarding the gPCE, we added the following reference to clarify the similarities with finite elements:

”R. Ghanem and J. R. Red-Horse. Propagation of probabilistic uncertainty in complex physical systems using a stochastic finite element technique. *Physica D*, 133:137144, 1999.”

Another reference has been added to clarify how the expansion coefficients are calculated and how the Clenshaw-Curtis quadrature is used:

”Eldred, M. & Burkardt, J. Comparison of non-intrusive polynomial chaos and stochastic collocation methods for uncertainty quantification AIAA paper, 2009, 976, 1-20”

For the comparison of the LHS and gPCE approaches, the number of runs has been chosen using the values suggested in the DAKOTA user manual. We have done additional tests with a smaller sample size (500 simulations) and we report here the results for the cumulative distribution function of the Solid Mass Flux Fraction Lost (see figure above). UQ results clearly show the error in using 500 runs and that a large number of simulations ( $\geq 1000$ ) is needed to reach a convergence of the results when the LHS approach is adopted.

**R1.** *Section 5.4: (i) The details of the sensitivity analysis should be given, or suitable references provided (e.g. Saltellis Sensitivity Analysis book, Sobol and Saltellis papers on this topic). (ii) The technical definitions in terms of*

variance of the conditional expectation are not intuitive to non-statisticians.

**A.** A reference to the following book has been added:

Saltelli, A.; Ratto, M.; Andres, T.; Campolongo, F.; Cariboni, J.; Gatelli, D.; Saisana, M. & Tarantola, S. Global sensitivity analysis: the primer John Wiley & Sons, 2008

**R1.** *Conclusion: Although only 91 simulations are required in the gPCE method applied to the plume model, I suspect that if the response function were not as smooth and well-behaved as for this model, many more model evaluations would be required. Furthermore, if more parameters were varied, the computational cost would increase for gPCE (and for LHS, although the advantage of gPCE might be reduced). Therefore, I feel there is an over-emphasis on the effectiveness of gPCE. In addition, is the computational saving enough to require the additional technical computations necessary? there is a cost in code development time for gPCE that is significantly greater than LHS.*

**A.** The referee is right when he says that if more parameters were varied, the computational cost would increase for gPCE, and this is now stated in the text. Conversely, the computational cost of the gPCE is negligible compared to the cost of the simulations, and thus there are no significant advantages in using the LHS.

**R1.** *Figure 1: The cross-section of the plume is circular in a plane normal to the centreline of the plume. This isnt clear on the diagram.*

**A.** The figure has been modified accordingly to the suggestion of the referee. we hope the figure is clearer now.

**R1.** *Figure 2: The axes in the plots dont seem appropriate. The top plot has a range for the Particle number distribution from  $10^{-50}$  to  $10^{+50}$ , which seems extremely large. Furthermore, the top plot suggests there are particles erupted with diameter in excess of  $10^7$  m! I suspect the labelling of the axis has gone wrong (missing minus sign in the indices?) and the particle diameter decreases to the right? The phi scale labels are also wrong.*

**A.** The range for the Particle number distribution from  $10^{-50}$  to  $10^{+50}$  is correct, but the problem, as noted by the referee, is that on the x-axis the minus sign have disappeared, bot in the exponents of the diameters expressed in meters and the diameters expresses in the phi scale. The corrected figure is presented here.

**R1.** *Figure 6: A fair comparison of the two sampling strategies would be to have 81 points in LHS sample as well as the Clenshaw-Curtis grid.*

**A.** The number of points for the sampling strategies presented in figure 6 does not have any reference to the simulations performed but it has only been chosen to clearly present the strategies. Using 81 points with the LHS would mean to partition both the x and y axis in 81 stripes and it would make really difficult the readability of the figure. On the other side, using less points for the Clenshaw-Curtis grid would not highlight enough how the points are distributed in the domain.

**R1.** *Figure 9: The sensitivity indices displayed for the Top panels cannot be correct. The response surfaces in figure 7 and 8 show that the contours of*

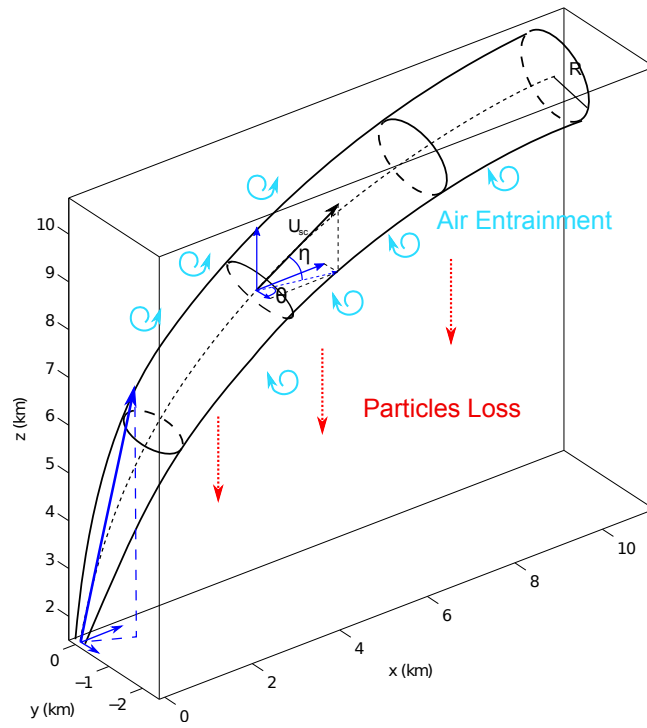


Figure 2: Schematic representation of the Eulerian plume model. The dashed black line represent the axis of the curvilinear coordinate  $s$ .



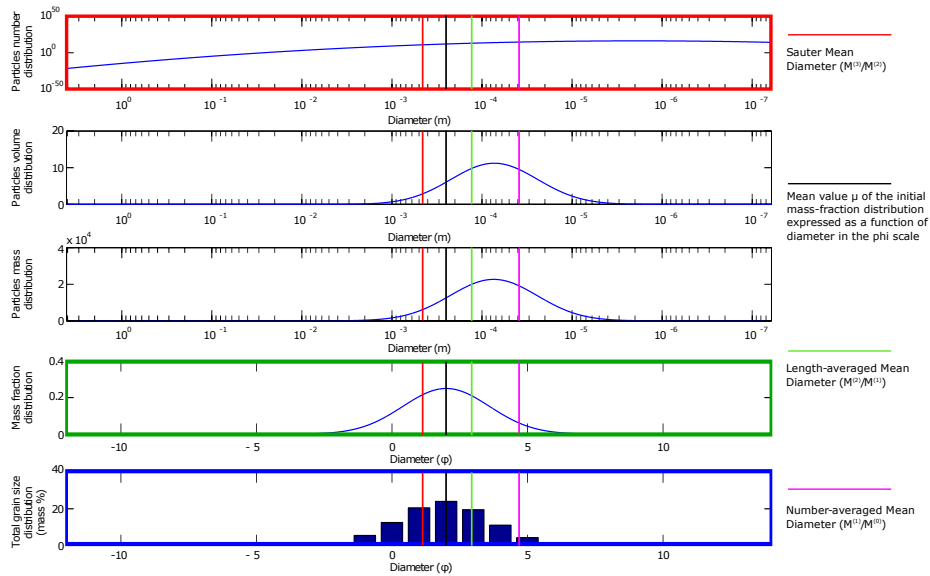


Figure 3: Visualization of a normal initial distribution in the Krumbein  $\phi$  scale for the solid particles.

*Top are not absolutely parallel Bottom , so there must be some sensitivity to the Bottom .*

**A.** The sensitivity indexes are correct. We remark here that the fact that the subplots in figure 7 and 8 are vertically stretched, and this could give the idea that there is a sensitivity to the parameter on the vertical axis larger than the real value. In any case the values of the sensitivity indexes, as computed from DAKOTA for Test case 2 and plotted in Figure 9 for "Top  $\sigma$ ", are reported here:

Global sensitivity indices for each response function:

response\_fn\_2 Sobol indices:

	Main	Total	
	3.7227494471e-04	1.2250701556e-03	x1
	9.9877492984e-01	9.9962772506e-01	x2
Interaction			
	8.5279521094e-04		x1 x2

We also report the coefficients of the polynomial expansion, from which it is possible to plot the contours and to evaluate analytically the sensitivity indices.

Polynomial Chaos coefficients for response\_fn\_2:

coefficient	u1	u2
-----	----	----
1.4336940817e+00	P0	P0
1.6578858566e-02	P1	P0
-2.5910899091e-03	P2	P0
-2.8116627135e-03	P3	P0
-3.2804547607e-04	P4	P0
6.7952933063e-03	P5	P0
-4.1395975864e-03	P6	P0
-2.9026509458e-03	P7	P0
-1.7098830327e-03	P8	P0
8.9814284834e-01	P0	P1
3.7262764551e-02	P1	P1
7.5125408867e-03	P2	P1
-1.6321040394e-02	P3	P1
2.2132291023e-03	P4	P1
5.8756408728e-04	P5	P1
5.7838688541e-03	P6	P1
1.1995615562e-03	P7	P1
-7.4673637468e-03	P8	P1
-4.1668082838e-02	P0	P2
2.3065350042e-02	P1	P2
2.3825461814e-03	P2	P2
2.1148501070e-03	P3	P2
1.7727374651e-03	P4	P2
-8.8478841637e-03	P5	P2
1.4551374661e-02	P6	P2
-3.8051790789e-03	P7	P2
1.8463422687e-03	P8	P2
-4.0920148065e-03	P0	P3
-1.6905356585e-03	P1	P3
-4.9839259871e-03	P2	P3
3.8944263097e-03	P3	P3
1.9329513445e-04	P4	P3
1.0878441090e-02	P5	P3
-8.6680149485e-03	P6	P3
-2.2863854848e-03	P7	P3
-5.4586661825e-04	P8	P3
2.2886609083e-03	P0	P4
-2.7465458556e-03	P1	P4

-3.0891928498e-03	P2	P4
-1.4646650257e-03	P3	P4
-4.7270771933e-03	P4	P4
1.2163990228e-03	P5	P4
-1.3854824406e-02	P6	P4
8.6678617316e-03	P7	P4
-6.7466120712e-04	P8	P4
1.1657009672e-04	P0	P5
4.9090095451e-03	P1	P5
3.7946796588e-03	P2	P5
-2.9495112304e-03	P3	P5
-4.1482366786e-04	P4	P5
-9.5659085116e-03	P5	P5
7.6261697982e-03	P6	P5
-2.9319826609e-03	P7	P5
7.1749457251e-03	P8	P5
-5.7901135737e-04	P0	P6
-3.0281356063e-03	P1	P6
4.2719008039e-03	P2	P6
1.7583283179e-03	P3	P6
8.3201878659e-03	P4	P6
2.6704665368e-03	P5	P6
1.2441515329e-02	P6	P6
-4.0571117721e-03	P7	P6
-9.6858649511e-03	P8	P6
-1.0293447697e-03	P0	P7
-3.7909388725e-03	P1	P7
-3.4938230431e-04	P2	P7
1.7733592128e-03	P3	P7
-4.2099940377e-04	P4	P7
6.0366622193e-03	P5	P7
-7.3902454998e-03	P6	P7
2.8979716727e-03	P7	P7
-5.2051392647e-04	P8	P7
1.4606844135e-03	P0	P8
7.3041710628e-03	P1	P8
-9.1532601056e-03	P2	P8
-9.8399168578e-04	P3	P8
-1.0310831209e-02	P4	P8
-6.2875060428e-03	P5	P8
-6.4367915934e-03	P6	P8
-6.2543284009e-04	P7	P8
1.0071554844e-02	P8	P8

**R1.** *Technical corrections*

**A.** We have considered all the corrections suggested by the referee modifying

the manuscript when appropriate.

## Responses to Referee 2

**R2.** *In the Introduction, your description of the value of using a continuously variable function is too vague to present a clear image of the problem and its importance. Much of problem is in a single sentence on lines 12-14 of page 3747, which describes the limitations of models that do not use continuously variable functions. I would change this line by deleting the . . . in the following: Both approaches make proper treatment of the continuous variability . . . of particles and gas bubbles difficult.*

**A.** We have modified the text as suggested by the referee and added a few more references.

**R2.** *In Section 2, it would be worthwhile adding a qualitative statement at the beginning or end of this section saying how the number-based moments, Sauter mean diameter in particular, differ from corresponding moments calculated by mass-based methods. The Sauter mean diameter appears to be an average diameter based on the number of particles rather than mass. Because there are more small particles than big ones, this mean diameter should be less than a mass-based mean diameter. Is this correct? Would the same apply for the moments of density and other properties?*

**A.** The Sauter mean diameter is not defined as a function of the number of particles but it is defined as the ratio between total volume and total surface area, where the total values are obtained integrating over all the particles. The fact that there are more small particles than big ones results in the fact that the diameter  $L_{10} = M^{(1)}/M^{(0)}$ , based on the number of particles of the different sizes (represented by  $M^{(0)}$ ), will be smaller than the diameter  $L_{43} = M^{(4)}/M^{(3)}$ , based on the volumes of the particles (proportional to  $M^{(3)}$ ). To clarify we added this physical interpretation also in the text.

**R2.** *A few key assumptions of the model should be stated more explicitly. For example I could see from the energy equation that phase changes in water were not considered, but I didnt see this point explained in the text.*

**A.** The main assumption of the model now are stated more explicitly at the beginning of Section 3: "In this section we describe the assumption and the equations of the model. As in Bursik 2001, the model assumes an homogeneous mixture of particles and gases with thermal and mechanical equilibrium between all phases. Aggregation and breakage effects are not considered and consequently density does not change with time. Finally, the model does not consider effects of humidity and water phase changes."

**R2.** *Page 3747: Lines 12-13: deleting of fundamental physical and chemical properties of the dispersed phases will make this sentence more concise and meaningful. Lines 14-19: could you cite some of the literature that you say makes the point in this sentence? Line 24: Many readers (including me) will be unfamiliar with the method of moments. What fundamental physical quantities are balanced in a population balance equation? And what are moments in physical terms? A general statement relevant to the Introduction. I am familiar with only one other 1-D plume model that treats the GSD as a continuous function and analyzes its change with height. Veitch and Woods [2001] looked*

*at changes in the GSD with height in a plume due to particle aggregation. Veitch and Woods isnt mentioned in this paper, but perhaps should be. Could one modify PlumeMom to calculate changes in GSD due to aggregation? This might be a selling point of this approach, since particle aggregation has proven very hard to model quantitatively by other methods.*

**A.** We removed the text as suggested by the referee. The following references have been added:

Costa, A.; Folch, A. and Macedonio, G. A model for wet aggregation of ash particles in volcanic plumes and clouds: 1. Theoretical formulation Journal of Geophysical Research: Solid Earth (1978–2012), 2010, 115.

Pal, R. Rheological behavior of bubble-bearing magmas Earth and Planetary Science Letters, 2003, 207, 165-179.

Llewellyn, E. W.; Mader, H. M. and Wilson, S. D. R. The constitutive equation and flow dynamics of bubbly magmas Geophysical Research Letters, 2002, 29.

More details on the moments and their physical interpretation have been added both in the introduction and further in the text.

Also in Veitch and Woods the GSD is not treated as a continuous function. This is explained in their appendix A.3: "To determine the evolution of the particle size distribution in the plume, we discretize the range of particle sizes and evaluate  $g(j)$  for integer values of  $j$  only."

Regarding the modification to the code to calculate changes in GSD due to aggregation, this is something that we are currently implementing in the model, and we agree with the referee that it is a selling point of the approach. This has been added in the abstract and conclusions.

**R2.** *page 3748, line 7: what do you mean by the implementation of the quadrature? Line 10: Uncertainty in what? What physical properties are you studying, whose uncertainty you want to incorporate?*

**A.** Part of text was missing. Now the text is "the implementation of the quadrature method of moments" and a reference has been added. The text has been extended writing "epistemic uncertainty in input parameters (characterizing lack-of-knowledge)".

**R2.** *Page 3749: Equation 1: What terms on the right-hand side of this equation are different for different moments? It seems that this  $f_j(D)$  would have to be different, but its not clear to me how. Also, perhaps mention that the second and third moment assume a spherical shape. Or if this is not the case, what do they assume? And what does the superscript  $i$  on  $D^i$  mean? Line 20: it would be helpful to explain briefly what the Sauter mean diameter means physically. I thought this was a diameter based on number concentration of particles but in Fig. 2 it shows the Sauter mean diameter as being larger than the mass-based mean, which one would not expect from a numbers-based diameter.*

**A.** The term on the right-hand side changing for different moments is the exponent  $i$  in  $D^i$ . The text has been changed clarifying the assumption of spherical particles for the expressions of the moments. The Sauter diameter is not based on number concentration but it is defined as the ratio between total

volume and total surface area. To clarify we added this physical interpretation also in the text.

**R2.** Page 3750: line 14: add such before as settling velocity. line 15: change function to functions.

**A.** We changed the text as suggested by the referee.

**R2.** Page 3751: Equation 3: actually, using the method of Bonadonna and Phillips, density at diameters intermediate between  $D1$  and  $D2$  are interpolated on a log scale of  $\phi$ , not on a linear scale of  $D$  as this equation indicates. Equation 4: what is the physical meaning of the different moments of density? Line 8: What are  $D^*$  and  $\rho^*$ ? Lines 11- 12: you define volumetric averaged density as the mass of particles per unit volume. Does per unit volume mean per unit volume in the jet or plume? Per unit volume of each particle? If per particle (as implied later), perhaps say "average mass per unit volume of particles"

**A.** Eq. 3 has been removed to avoid confusion and the text has been changed in the following way: "density of pumices  $\rho_{s,pum}(D)$  with diameter  $< 2$  mm is assumed to decrease and to reach the lithic density value when the fragment diameter decreases below  $8 \mu\text{m}$ ."

The physical meaning of the different moments of density is explained in the text: "Otherwise, there is no reason, e.g., for  $\rho_{s,j}^{(1)}$  and  $\rho_{s,j}^{(3)}$  to be the same, as they represent length and volume weighted density averages, respectively." This means that the moment of order 1 is an average with a weight given by the particle length, the third moment is an average with the weight given by the volumes. In the same way, for example, the moment of order zero will just integrate the densities and divide by the total number of particles.

$D^*$  and  $\rho^*$  are the constant values assumed for a monodisperse distribution. This has been now clarified in the text.

The referee is right and the definition has been corrected writing "average mass per unit volume of particles".

**R2.** Page 3752: line 10: Put Pfeiffer et al. (2005); Textor et al. (2006a, b) in parentheses. Equation 8: what is the physical meaning of the moments of settling velocity? Maybe this could be addressed by just moving the statement (line 3 of the next page) that they represent surface and volume-weighted averages to the line immediately above the equation.

**A.** The parentheses have been added. The physical meaning of the different moments is simply a different way to evaluate the weighted average, i.e. weighting the settling velocities of particles of different sizes with a quantity proportional to the particle surface ( $D^2$ ) or to the particle volume ( $D^3$ ).

**R2.** Page 3753: Line 5: change particles to particles, to make it possessive.

**A.** Done!

**R2.** Page 3756: Line 13-14: bulk density means mass of particles per unit volume of particles? Mass of particles per unit volume of plume mixture? If the latter, maybe say mass of particles per unit volume of plume mixture, or something similar.

**A.** The definition has been added to the text: "bulk density of the particles of the  $j$ -th family (i.e. the mass of particles of the  $j$ -th family per unit volume

of gas-particles mixture)”.

**R2.** *Page 3757: Equations 22, 23: If this is a 3-D coordinate system, shouldn't there be three momentum conservation equations? Also, in the equation for horizontal momentum (22), I've generally thought of the change in momentum of the gaseous phase (first term on the right-hand side) as being equal to the horizontal momentum contained in the entrained air ( $2*r*rho_{atm}*U_e*w$ ). Your formulation is a little different. Perhaps you could add a sentence explaining your formulation.*

**A.** As stated in the introduction, in this work we present an extension of the Eulerian steady-state volcanic plume model presented in Barsotti et al. (2008) (derived from Bursik, 2001). Eqs. 22 and 23 use the same formulation of Eqs. 4 and 5 in Barsotti et al. (2008), with the only difference that the loss of particles is computed in terms of the moments. The reference to the original work has now been added to the text.

**R2.** *Page 3758: Equation 24 (energy equation): Do you mention anywhere that you are not considering phase changes of water? It looks from this equation like you are not considering it, but I don't see that you mention this point in the anywhere in the text. Line 18: What do the superscript Bs represent? Also, defining the rho terms on this line as bulk densities seems misleading (at least to me). In order for the denominators on the top and bottom of eq. 26 to be consistent, the rhos must be the mass (or air, water vapor etc.) per unit volume plume mixture, not per unit volume of air or water vapor. Perhaps refer to them as the mass of each component per unit volume of plume fluid. (maybe I missed it).*

**A.** A paragraph has been added at the beginning of the section where the main assumptions, as the fact that we are not considering phase change of water, are listed. The superscript  $B$  is used for the bulk properties and now it is defined in the text when the bulk density is introduced. As stated before, the bulk density refers to the mass of a phase per unit volume of the mixture, and thus the definition given by Eq.26 is consistent with the interpretation given by the referee.

**R2.** *Page 3760: Line 15: change particles number to particle numbers*

**A.** The text has been changed.

**R2.** *Page 3762: Equation 40: If these are ODEs, the LHS of eq. (40) should be  $dy/ds$  rather than  $\partial(y)/\partial(s)$ . Equation 41: perhaps add a multiplication symbol on the RHS between  $ds$  and  $f()$ .*

**A.** The partial derivatives have been changed to  $dy/ds$ .

**R2.** *Page 3764: Line 14 and elsewhere: change particles family to particle family Line 23: change particles size distribution to particle size distribution*

**A.** The text has been changed.

**R2.** *Page: 3765: Line 9: change “then writes as” to “is then written as” Equations 44: does  $\log_2$  mean the log base 10 of 2? Maybe write as  $\log_{10}(2)$ . Or, if you mean the natural log, then write  $\ln(2)$ . Pages 3765-3768: this is quite a slog through this section. Its not clear exactly where you're going. Adding a sentence at the beginning of Section 4.2.1 stating your objective in deriving these formulas might help readers keep their interest.*



**A.** “then writes as” has been changed to “is then written as”. All the occurrences of “log” have been changed to “ln”. Furthermore, a sentence has been added before the subsection 4.2.1 to better introduce what is the objective in deriving the formulas.

**R2.** *Page 3769: Line 5: the term “weak plume without wind” makes no sense to me, since a weak plume is generally defined as one that is bent over by wind [Sparks et al., 1997, p. 279]. “Low-flux plume without wind” may be more accurate. Line 16: you use a normal distribution? Not lognormal? Line 13: can you provide a reference for the standard atmosphere cited here? Line 17: change “expresses” to “expressed”. Line 18: Are you describing three different model runs, or a single model run with the output portrayed in three different ways?*

**A.** The text has been changed using the term suggested by the referee “Low-flux plume without wind”. The normal distribution is referred to the phi scale, it is a lognormal when the diameter is expressed in meters. A reference for the standard atmosphere has been added:

“Champion, K.; Cole, A. & Kantor, A. Standard and reference atmospheres Handbook of Geophysics and the Space Environment, Air Force Geophysics Laboratory, 1985, 14”

In the figure we present three different model runs with the same initial condition, but with different modeling approaches used to describe the GSD: discretization in bins, moments of the number of particles as a function of diameter expressed in meters, moments of the mass fraction of particles expressed as a function of the diameter expressed in the phi scale.

**R2.** *Page 3772: a nicely written and illuminating summary of the Latin Hypercube and gPCE alternatives to MCMC modeling.*

**A.** Thank you!

**R2.** *Page 3773: Still illuminating. Im not a specialist in the mathematics of these techniques and cant critique them. Its a little unclear to me what the form of equation 55 would be if fully expanded. For example, if zeta were a vector of 3 variables, would P1 represent three families of polynomial coefficients; one for each variable?*

**A.** Thank you again for the positive comment. Some references have been added where the technique is explained in more details. If zeta were a vector of 3 variables, P1 would be a polynomial of the 3 variables. The polynomials P1,P2,...Pn have to be orthogonal, i.e. the integral of the product of two polynomials with index i and j (with  $i \neq j$ ) has to be equal to zero.

**R2.** *Page 3774: the values contoured in the lower panels of Fig. 7 were not initially very clear to me. You call them response functions in the caption, and on page 3773 (line 17). Are these the values of gamma(zeta) in eq. 55? Perhaps referring to gamma(zeta) as a response function would clarify. Also, it would help to mention that the values contoured in the lower panels are the same as those plotted in the upper panels (e.g. top mean phi for panel 1). Lines 22-30: I would say that the points you make in these few lines are the most significant of the paper, for readers interested in geologically relevant findings.*

**A.** As suggested by the referee, we refer now to eq.55 when presenting the

response functions. We also added that the values contoured in the lower panels are the same as those plotted in the upper panels: "The variables contoured in the lower panels are the same as those on the horizontal axes in the upper panels".

**R2.** *Page 3775: Line 4: change reduce to reduces. Line 5: change relevance to relevance. Line 6: change entrained aid to entrained air. lines 13-14: The mean and the SD of the TGDS at the top of the eruptive column clearly reflects the corresponding values at the bottom, with a small effect on the mean size at the top of larger values of the bottom SD. What does this mean?*

**A.** All the typos have been corrected. The sentence was really confusing and it has been rephrased in the following way: "a small effect of the bottom standard deviation on the mean size at the top, resulting in an increase in the average grain size with increasing values of the initial standard deviation".

**R2.** *Page 3776: Line 10: Im a little confused about which of the sensitivity indices ( $S_i$  or  $T_i$ ) is displayed in Fig. 9.*

**A.** The indices plotted are the main indices  $S_i$ . This is now written in the caption of figure 9.

**R2.** *Figure 2 caption, line 4: change forth to fourth. Figure 5: the light gray curves on this figure are hard to see on my computer screen. Darkening them should make them more visible. Figure 6 caption: change Two parameters Latin Hypercube to Two-parameter Latin Hypercube*

**A.** The caption of figure 2 has been corrected. In Figure 5 now the lines are more visible. The caption of figure 6 has been corrected.

### Responses to Referee 3

**R3.** *In Section 5.3 5.4, the logic is complicated and messy, and there are many technical jargons that are not defined nor fully explained. Response surface is not clearly de- fined, and therefore, it is difficult to understand Figs. 7 and 8. For these uncertainty and sensitivity analysis, more systematic parameter study is required using a lot of simula- tion settings such as vent and atmospheric conditions to obtain the general conclusion about a small change of the size distribution along the plume. In my opinion, in order to clarify the focus of this paper, it is better to describe the discussion of Section 5.3 5.4 in another paper after thorough analyses and discussion.*

**A.** Accordingly to the suggestions of the referees, we have tried to clarify some of the terms used, as "response surface" and more references have been added. For the uncertainty and sensitivity analysis, a more systematic parame- ter study was out of the scope of this paper. This is actually the main topic of a parallel papaer we are working on. Our aim here was to apply the sensitivity analysis and uncertainty quantification techniques to the parameters described by the moments of the particle size distribution, since the paper focuses on this specific issue. Sections 5.3 and 5.4 also provide informations on the changes in the parameters describing the grain size distribution for the three different test cases, otherwise presented only in Figure 5. For these reasons, we do not think that the content of the sections should be moved in another paper but that it helps in generalizing the results presented in Sections 5.1 and 5.2.

**R3.** *p.3755, Eq.(16): It needs a reference that clearly expresses the formu- lation. For example, Bursik et al. (1992).*

**A.** The reference has been added.

**R3.** *p.3759, Eq.(28): In order to evaluate this equation, it will be helpful to briefly describe the derivation from Eq.(26) to Eq.(28) in appendix.*

**A.** I've reported here the steps for the derivation of the equation. There is nothing particularly interesting because it mostly consists in expanding the derivatives and rearranging and canceling some terms. For this reason we do not think that there should be an appendix, but if the referees and the editor thinks that this would be helpful, we can add these steps in an appendix.

$$C_{mix} = \frac{\rho_{atm}^B C_{atm} + \rho_{wv}^B C_{wv} + \sum_j \rho_{s,j}^B \bar{C}_{s,j}}{\rho_{atm}^B + \rho_{wv}^B + \sum_j \rho_{s,j}^B}. \quad (1)$$

From this expression, if we multiply all the terms at the numerator and the

denominator of the right-hand side by  $U_{sc}r^2$ , and then we derive, we obtain:

$$\begin{aligned} & \frac{\partial C_{mix}}{\partial s} = \\ & \left[ \frac{C_{atm}}{(\rho_{atm}^B + \rho_{wv}^B + \sum_j \rho_{s,j}^B)U_{sc}r^2} - \frac{\rho_{atm}^B C_{atm} + \rho_{wv}^B C_{wv} + \sum_j \rho_{s,j}^B \bar{C}_{s,j}}{(\rho_{atm}^B + \rho_{wv}^B + \sum_j \rho_{s,j}^B)^2 U_{sc}r^2} \right] \frac{\partial}{\partial s} [\rho_{atm}^B U_{sc}r^2] \\ & + \sum_j \left[ \frac{\bar{C}_{s,j}}{(\rho_{atm}^B + \rho_{wv}^B + \sum_j \rho_{s,j}^B)U_{sc}r^2} - \frac{\rho_{atm}^B C_{atm} + \rho_{wv}^B C_{wv} + \sum_j \rho_{s,j}^B \bar{C}_{s,j}}{(\rho_{atm}^B + \rho_{wv}^B + \sum_j \rho_{s,j}^B)^2 U_{sc}r^2} \right] \frac{\partial}{\partial s} [\rho_{s,j}^B U_{sc}r^2] \\ & + \sum_j \frac{\rho_{s,j}^B U_{sc}r^2}{(\rho_{atm}^B + \rho_{wv}^B + \sum_j \rho_{s,j}^B)U_{sc}r^2} \frac{\partial \bar{C}_{s,j}}{\partial s} \end{aligned} \quad (2)$$

Now, we obtain after the collection of some terms and some algebra manipulations the following equation for the variation of the mixture specific heat with  $s$ :

$$\begin{aligned} & \frac{dC_{mix}}{ds} = \\ & \frac{1}{\rho_{mix}U_{sc}r^2} \left[ (C_{atm} - C_{mix}) \frac{d}{ds} (\rho_{atm}^B U_{sc}r^2) \right. \\ & \left. + \sum_j (\bar{C}_{s,j} - C_{mix}) \frac{d}{ds} (\rho_{s,j}^B U_{sc}r^2) \right] \\ & + \sum_j \frac{\rho_{s,j}^B}{\rho_{mix}} \left[ \frac{d}{ds} (\bar{C}_{s,j} \rho_{s,j}^B U_{sc}r^2) - \bar{C}_{s,j} \frac{d}{ds} (\rho_{s,j}^B U_{sc}r^2) \right]. \end{aligned} \quad (3)$$

Finally, with some cancellation:

$$\begin{aligned} & \frac{\partial C_{mix}}{\partial s} = \\ & \frac{1}{\rho_{mix}U_{sc}r^2} \left[ C_{atm} \frac{\partial}{\partial s} (\rho_{atm}^B U_{sc}r^2) \right. \\ & \left. - C_{mix} \left( \frac{\partial}{\partial s} (\rho_{atm}^B U_{sc}r^2) + \frac{\partial}{\partial s} (\rho_s^B U_{sc}r^2) \right) + \frac{\partial}{\partial s} (\bar{C}_s \rho_s^B U_{sc}r^2) \right] \end{aligned} \quad (4)$$

and, substituting the expressions for the partial derivatives appearing in each term on the right-hand side:

$$\begin{aligned} \frac{dC_{mix}}{ds} = & \frac{1}{\rho_{mix}U_{sc}r^2} \left[ C_{atm}2r\rho_{atm}U_{\epsilon} - C_{mix} \left( 2r\rho_{atm}U_{\epsilon} \right. \right. \\ & \left. \left. - 2pr \sum_j \frac{\pi}{6} M_j^{(3)} [w_{s,j}\rho_{s,j}]^{(3)} \right) \right. \\ & \left. - 2pr \sum_j \frac{\pi}{6} M_j^{(3)} [w_{s,j}\rho_{s,j}C_{s,j}]^{(3)} \right] \end{aligned} \quad (5)$$

**R3.** *p.3760, Eq.(30): It is also required to describe the derivation from Eq.(29) to Eq.(30) in appendix.*

**A.** The steps are the same used for the previous equation.

**R3.** *Section 4.1: For researchers in volcanology community, this section is quite difficult to understand. In order to clarify the algorithm, the wording and style of this section need careful editing. What are the meanings of realizable and unrealizable?*

**A.** We have tried to simplify this section removing some part and adding some reference. For the meaning of the term "realizable", this was explained in the text at pag.3763, lines 20-21:

"the moment set is realizable, meaning that there exists a particle size distribution resulting in that specific set of moments."

Conversely, unrealizable set of moments means that there are no distributions resulting in that specific set of moments. In any case, we moved the definition before in the text, to make it clearer.

**R3.** *p.3770, paragraph from line 20: Usually, the variation of distribution is also evaluated by kurtosis. The skewness has a peak value at about 2 km and decreases with height. What do these features of the skewness at the lower region of plume mean?*

**A.** We agree that also the kurtosis is used to characterize distributions, and it can be obtained from the moments (as now written in the text) but the changes in the values are more difficult to interpret in the context of a particle size distribution. The same difficulty in the interpretation apply to the value of the skewness.

**R3.** *Section 5.2: We would like to see the variations of size distributions for Cases 1 and 3 like Figure 5. It is better to carefully describe the similarity and difference between the cases on the basis of these figures. In addition, it will be helpful to show the variation of 2-D distributions in the horizontal spaces.*

**A.** We report below the plots obtained for Cases 1 and 3. We remark that the outcomes of these plots, i.e. the changes in the mean and SD of the grain size distribution and the solid mass flux fraction lost, are consistent with the results already presented in figure 7 and 8, and discussed in the manuscript. Only the variations of skewness is not presented in figs. 7 and 8 but, as stated in the answer to the previous comment, the changes in the skewness are difficult

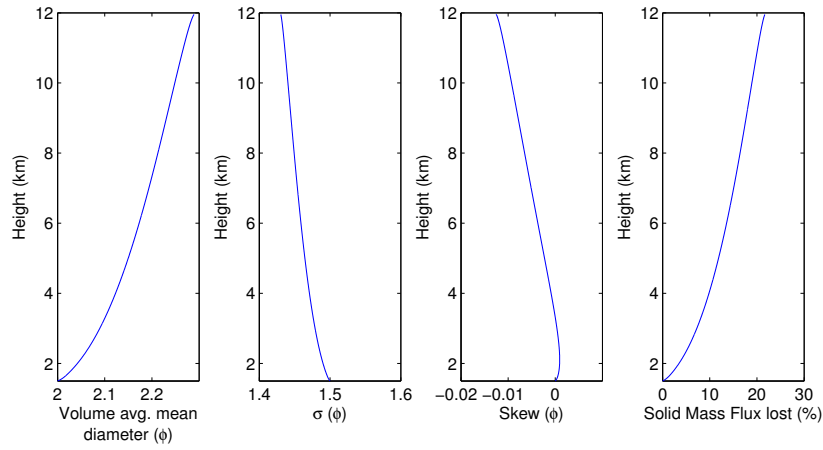


Figure 4: Particles distribution parameters (mean, variance and skewness) and cumulative loss of solid mass flux for test case 1.

to interpret and also quite small, in particular for the strong plumes. Regarding the 2-D distributions in the horizontal spaces, the model assumes a top-hat profile so there are not variations in the cross-sectional plane orthogonal to the plume centerline.

**R3.** *p. 3786, caption of Figure 5: The caption should clearly indicate that these figures are the results of Case 2.*

**A.** Done.

**R3.** *Technical corrections*

**A.** All the corrections suggested by the reviewer have been done.

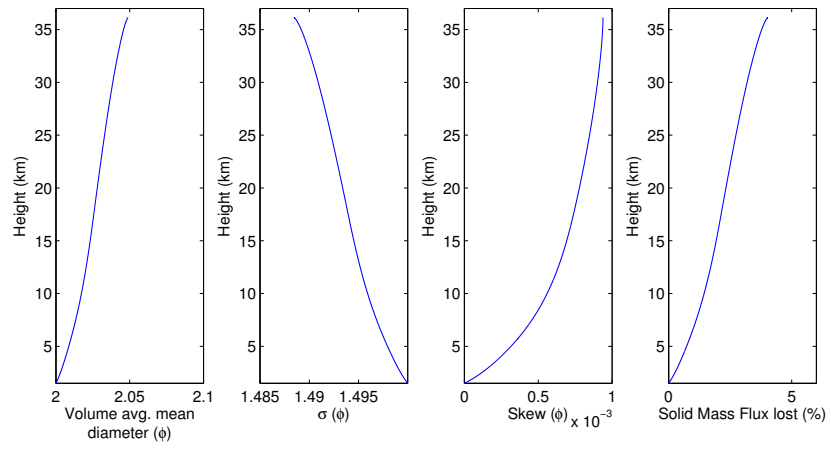


Figure 5: Particles distribution parameters (mean, variance and skewness) and cumulative loss of solid mass flux for test case 3.

# PLUME-MoM 1.0: A new **integral** model of volcanic plumes based on the method of moments

Mattia de' Michieli Vitturi<sup>1</sup>, Augusto Neri<sup>1</sup>, and Sara Barsotti<sup>2</sup>

<sup>1</sup>Istituto Nazionale di Geofisica e Vulcanologia, Sezione di Pisa, Italy

<sup>2</sup>Icelandic Meteorological Office, Reykjavík, Iceland

*Correspondence to:* M. de' Michieli Vitturi (mattia.demichielivitturi@ingv.it)

## Abstract.

In this paper a new **integral** mathematical model for volcanic plumes, named PlumeMoM, is presented. The model describes the steady-state dynamics of the plume in a 3D coordinate system, accounting for continuous variability in particle **size** distribution of the pyroclastic mixture ejected at the vent. Volcanic plumes are composed of pyroclastic particles of many different sizes ranging from a few microns up to several centimeters and more. Proper description of such a multiparticle nature is crucial when quantifying changes in grain-size distribution along the plume and, therefore, for better characterization of source conditions of ash dispersal models. The new model is based on the method of moments, which allows description of the pyroclastic mixture dynamics not only in the spatial domain but also in the space of parameters of the continuous size-distribution of the particles. This is achieved by formulation of fundamental transport equations for the multiparticle mixture with respect to the different moments of the grain-size distribution. Different formulations, in terms of the distribution of the particle number, as well as of the mass distribution expressed in terms of the Krumbein log scale, are also derived. Comparison between the new moments-based formulation and the classical approach, based on the discretization of the mixture in N discrete phases, shows that the new model allows the same results to be obtained with a significantly lower computational cost (particularly when a large number of discrete phases is adopted). Application of the new model, coupled with uncertainty quantification and global sensitivity analyses, enables investigation of the response of four key output variables (mean and standard deviation of the grain-size distribution at the top of the plume, plume height and amount of mass lost by the plume during the ascent) to changes in the main input parameters (mean and standard deviation) characterizing the pyroclastic mixture at the base of the plume. Results show that, for the range of parameters investigated **and without considering interparticle processes such as aggregation or comminution**, the, the grain-size



distribution at the top of the plume is remarkably similar to that at the base and that the plume height is only weakly affected by the parameters of the grain distribution. The adopted approach can be potentially extended to the consideration of key particle-particle effects occurring in the plume including particle aggregation and fragmentation.

## 1 Introduction

In the past decades, numerical simulation of volcanic eruptions has greatly advanced and models are now often able to deal with the multiphase nature of volcanic flows. This is the case, for example, of models describing the dynamics of pyroclastic particles in a volcanic plume, or that of bubbles and crystals dispersed in the magma rising in a volcanic conduit. Despite this, in numerical models, the polydispersity associated with the multiphase nature of volcanic flows is often ignored or largely simplified (Valentine and Wohletz, 1989; Neri et al., 2003; Darteville, 2003; Dufek and Bergantz, 2007; Esposti Ongaro et al., 2007; de' Michieli Vitturi et al., 2010). For instance, in most of the existing conduit models, crystals and bubbles are treated as simple flow components and described by volume fractions only, while in plume dynamics and ash dispersal models the grain size distribution of pyroclasts is discretized in a finite number of classes (i.e. phases). Both approaches make proper treatment of the continuous variability of the dimension of pyroclastic particles and gas bubbles difficult. Literature results (Llewellyn et al., 2002; Pal, 2003; Costa et al., 2010) clearly show that this variability can largely affect relevant physical/chemical processes that occur during the transport of the dispersed phase such as, for example, the nucleation and growth of bubbles and the coalescence/breakage of bubbles and crystals in the conduit or the aggregation of pyroclastic particles in a volcanic plume.

A theoretical framework and the corresponding computational models, namely the method of moments for disperse multiphase flows, have been developed in the past decades, mostly in the chemical engineering community (Hulburt and Katz, 1964; Marchisio et al., 2003), to track the evolution of these systems not only in the physical space, but also in the space of properties of the dispersed phase (called internal coordinates). According to this method, a population balance equation is formulated as a continuity statement written in terms of a density function. From the density function some integral quantities of interest (namely the moments, i.e. specific quantitative measures of the shape of the density function) are then derived and their transport equations are formulated.

In this work we present an extension of the Eulerian steady-state volcanic plume model presented in Barsotti et al. (2008) (derived from Bursik (2001)) obtained by adopting the method of moments. In contrast to the original works where pyroclastic particles are partitioned into a finite number of classes with different size and properties, the new model is able to consider a continuous size distribution function of pyroclasts,  $f(D)$ , representing the number or the mass fraction of particles

(per unit volume) with diameter between  $D$  and  $D + dD$ . Accordingly, conservation equations of  
60 the plume are expressed in terms of the transport equations for the moments of the ash particles size  
distribution. In particular in the following we present the new multiphase model formulation based  
on the implementation of the quadrature method of moments McGraw (2006) and we investigate the  
sensitivity of the model to uncertain or variable input parameters such as those describing the grain-  
size distribution of the mixture. To quantify and incorporate this epistemic uncertainty affecting the  
65 input parameters (characterizing lack-of-knowledge) into our application of the model we tested two  
different approaches, a modification of the Monte Carlo method based on Latin hypercube sampling  
and a stochastic approach, namely the generalized Polynomial Chaos Expansion method.

This paper is organized as follows: in Section 2 we present the method of moments applied to  
two different descriptions of particles distribution. In Section 3 the equations of the model for the  
70 two formulations are described. Section 4 is devoted to the numerical discretization of the model  
and the numerical implementation of the method of moments. Section 5 presents the application of  
the model to three test cases with a comparison of the model results for different formulations of  
the plume model, and finally an uncertainty quantification and a sensitivity analysis are applied to  
model results.

## 75 2 Method of Moments

### 2.1 Moments of the size distribution

In contrast to previous works, where the solid particles are partitioned in a finite number of classes  
with different size (Barsotti et al., 2008), we introduce here a continuous size distribution function  
representing the number (or mass) concentration of particles (per unit volume) as a function of the  
80 particles diameter. In general, this particle size distribution (PSD) is a function of time  $t$ , of the  
spatial coordinate and of the diameter of the particles.

First, we present the method of moments for a particle size distribution  $f(D)$ , representing the  
number concentration of particles (particles per unit volume) with diameter between  $D$  and  $D + dD$ ,  
where  $D$  is expressed in meters. When more than one family of particles are present, for example  
85 lithics and pumice, we will use the subscript  $j$  to distinguish among them. Consequently, the function  
 $f_j(D)$  will denote the number concentration of particles of the  $j$ -th family.

Given a particle size distribution  $f_j(D)$ , we observe that its “shape” can be quantified through the  
moments  $M_j^{(i)}$  (Hazewinkel, 2001), defined by

$$M_j^{(i)} = \int_0^{+\infty} D^i f_j(D) dD. \quad (1)$$

90 The particular definition of  $f_j(D)$  we adopt, expressing the number concentration of particles of  
size  $D$ , allows the following physical interpretation of the first four moments:

- $M_j^{(0)}$  is total number of particles of the  $j$ -th family(per unit volume);
- $M_j^{(1)}$  is sum of the particles diameter of the  $j$ -th family(per unit volume);
- $M_j^{(2)}$  is total surface area of particles of the  $j$ -th family(per unit volume);
- 95 –  $\frac{\pi}{6}M_j^{(3)}$ : total volume of particles of the  $j$ -th family (per unit volume) or the local volume fraction of the  $j$ -th dispersed phase, also denoted with  $\alpha_{s,j}$ . The multiplying factor  $\frac{\pi}{6}$  is obtained assuming spherical particles. For particles with different shape, if volume scales with the third power of length, we can still relate the particle volume  $V$  with the particle length  $D$  through a volumetric shape factor  $k_v$  such as  $V = k_v L^3$ .

100 We also note that the central moments (i.e., those taken about the mean) can be expressed as function of the raw moments (i.e., those taken about zero as in Eq. (1)), and in this way it is possible to relate the moments of the distribution with the mean, variance, skewness, kurtosis. Furthermore, a mean particle size can be defined as the ratio of the moments  $M_j^{(i+1)}/M_j^{(i)}$  for any value of  $i$ . For example, the Sauter mean diameter (defined as the ratio between the mean volume and the mean surface area) is obtained by setting  $i = 2$ , giving  $L_{j,32} = M_j^{(3)}/M_j^{(2)}$ . Similarly, it is possible to define the mean particle length averaged with respect to particle number density  $L_{j,10} = M_j^{(1)}/M_j^{(0)}$ , i.e. the sum of the lengths of particles (per unit volume) divided by the number of particles (per unit volume), and the mean particle length averaged with respect to particle volume-fraction  $L_{j,43} = M_j^{(4)}/M_j^{(3)}$ .

110 The motivation for the introduction of the moments is to minimize computational costs by avoiding the discretization of the size distribution in several classes, and nevertheless to capture the polydispersity of the flow through the correct description of the evolution of the moments (Carneiro, 2011). The moments approach also allows to treat interparticles processes such as particle aggregation and fragmentation that strongly depend on and affect the GSD of the mixture (Marchisio et al., 115 2003). The moments and the corresponding transport velocities appear naturally in the mathematical formulation as a direct consequence of the integration of the Eulerian particle equations over the diameter spectrum, as will be shown in the next section.

## 2.2 Moments of other quantities

In the plume model, several quantities characteristic of the particles, such as settling velocity, density 120 and specific heat capacity, are also defined as functions of the particle diameter, and thus we can define their moments as done for the particle size distribution  $f_j(D)$ . In general, for a quantity  $\psi_j$  that is a function of the diameter  $D$ , we define its moments as

$$\psi_j^{(i)} = \frac{1}{M_j^{(i)}} \int_0^{+\infty} \psi_j(D) D^i f_j(D) dD. \quad (2)$$

As a first example, we consider here the moments of particles density  $\rho_s$ . In particular, following Bonadonna and Phillips (2003), density of lithics is assumed to be constant, whereas density of pumices  $\rho_{s,pum}(D)$  with diameter  $D < D_2$  (here equal to 2 mm) is assumed to decrease and to reach the lithic density value when the fragment diameter decreases below  $D_1$  (here equal to 8  $\mu\text{m}$ ). Substituting the expression for the particles density of the  $j$ -th particle family in Eq. (2), we obtain the moments of the density as:

$$\rho_{s,j}^{(i)} = \frac{1}{M_j^{(i)}} \int_0^{+\infty} \rho_{s,j}(D) D^i f_j(D) dD. \quad (3)$$

We remark that moments of different order are generally different, they will only be equal ( $\rho_{s,j}^{(l)} = \rho_{s,j}^{(m)}$ ,  $l \neq m$ ) in two limiting cases: for a monodisperse distribution with diameter  $D^*$  and density  $\rho_s^*$ , i.e.  $f_j(D) = \delta(D - D^*)$  (where  $\delta$  is the Dirac-delta function) and  $\rho_{s,j}(D^*) = \rho_s^*$ ; or if all particles have the same density, i.e.  $\rho_{s,j}(D) = \rho_s^*$ ,  $\forall D$ . In both cases,  $\rho_{s,j}^{(i)} = \rho_s^*$ ,  $\forall i$ . Otherwise, there is no reason, e.g., for  $\rho_{s,j}^{(1)}$  and  $\rho_{s,j}^{(3)}$  to be the same, as they represent length and volume weighted density averages, respectively. For our application, we are interested mostly in the volumetric averaged density  $\rho_{s,j}^{(3)}$ , i.e. the average mass per unit volume of particles from now on denoted with  $\tilde{\rho}_{s,j}$ .

The moments defined by Eq. (3) can also be used to define other properties of the gas-particles mixture. For example, it follows from the definition of the moments that if we have a mixture of a gas with density  $\rho_g$  and a family of polydisperse distributions of particles with density  $\rho_{s,j} = \rho_{s,j}(D)$ , the mixture density is given by:

$$\begin{aligned} \rho_{mix} &= \sum_j \alpha_{s,j} \tilde{\rho}_{s,j} + (1 - \sum_j \alpha_{s,j}) \rho_g = \\ &= \sum_j \frac{\pi}{6} M_j^{(3)} \rho_{s,j}^{(3)} + (1 - \sum_j \frac{\pi}{6} M_j^{(3)}) \rho_g \end{aligned} \quad (4)$$

and consequently the mass fraction of the  $j$ -th solid phase with respect to the gas-particles mixture is given by:

$$x_{s,j} = \frac{\alpha_{s,j} \tilde{\rho}_{s,j}}{\rho_{mix}} = \frac{\frac{\pi}{6} M_j^{(3)} \rho_{s,j}^{(3)}}{\sum_j \frac{\pi}{6} M_j^{(3)} \rho_{s,j}^{(3)} + (1 - \sum_j \frac{\pi}{6} M_j^{(3)}) \rho_g}. \quad (5)$$

We also remark that here the gas phase is a mixture of atmospheric air, entrained in the plume during the rise in the atmosphere, and a volcanic gas component, generally water vapour. In the following, we will use the subscript *atm* to denote the atmospheric air and *wv* for the volcanic water vapour.

Differently from the approach used in Barsotti et al. (2008), where a constant settling velocity for each class is provided by the user, here several models have implemented in the code (Pfeiffer et al., 2005; Textor et al., 2006a, b). For the application presented in this work, the settling velocity

is defined as a function of the particle diameter and density as in Textor et al. (2006a):

$$w_{s,j}(D) = \begin{cases} k_1 \left(\frac{D}{2}\right)^2 \rho_{s,j}(D) \sqrt{\frac{\rho_{atm}^0}{\rho_{atm}}} & D \leq 10\mu m \\ k_2 \left(\frac{D}{2}\right) \rho_{s,j}(D) \sqrt{\frac{\rho_{atm}^0}{\rho_{atm}}} & 10 < D \leq 10^3\mu m \\ k_3 \sqrt{\frac{D}{2}} \sqrt{\frac{\rho_{s,j}(D)}{C_D}} \sqrt{\frac{\rho_{atm}^0}{\rho_{atm}}} & D > 10^3\mu m \end{cases} \quad (6)$$

where  $k_1 = 1.19 \times 10^5 \text{ m}^2\text{kg}^{-1}\text{s}^{-1}$ ,  $k_2 = 8 \text{ m}^3\text{kg}^{-1}\text{s}^{-1}$  and  $k_3 = 4.833 \text{ m}^2\text{kg}^{-1/2}\text{s}^{-1}$ . The drag coefficient  $C_D$  is a parameter accounting for the particles surface roughness, and for this work we used a value of 0.75 as in Carey and Sparks (1986).

Proceeding as done for the particle density, it is possible to evaluate the moments  $w_{s,j}^{(i)}$  of the settling velocity  $w_{s,j}(D)$ , defined as

$$w_{s,j}^{(i)} = \frac{1}{M_j^{(i)}} \int_0^{+\infty} w_{s,j}(D) D^i f_j(D) dD \quad (7)$$

and representing weighted integrals of the settling velocity over the size spectrum. Again, moments of different order are generally different. There is no reason, e.g., for  $w_{s,j}^{(2)}$  and  $w_{s,j}^{(3)}$  to be the same, as they represent surface and volume weighted averages, respectively.

Finally, it is possible to define the moments  $C_{s,j}^{(i)}$  of the particles' specific heat capacity  $C_{s,j}$ :

$$C_{s,j}^{(i)} = \frac{1}{M_j^{(i)}} \int_0^{+\infty} C_{s,j}(D) D^i f_j(D) dD. \quad (8)$$

We observe that for the specific heat capacity generally we are not interested in a volumetric average but in the mass average, denoted here with the notation  $\bar{C}_{s,j}$  and given by the following expression:

$$\bar{C}_{s,j} = \int_0^{+\infty} C_{s,j}(D) \frac{\rho_{s,j}(D) D^3}{\tilde{\rho}_{s,j} M_j^{(3)}} f_j(D) dD = \frac{1}{\tilde{\rho}_{s,j}} [C_{s,j} \rho_{s,j}]^{(3)}. \quad (9)$$

### 2.3 Mass fraction distribution

While in chemical engineering, where the method of moments is commonly used, the particle number distribution  $f_j(D)$  is generally preferred to describe the polydispersity of the particles, in volcanology it is more common to use a mass fraction distribution  $\gamma_j(\phi)$ , defined as a function of the Krumbein phi ( $\phi$ ) scale:

$$\phi = -\log_2 \frac{1000D}{D_0},$$

where  $D$  is the diameter of the particle expressed in meters, and  $D_0$  is a reference diameter, equal to 1 mm (to make the equation dimensionally consistent).

In this case, the distribution  $\gamma_j(\phi)$  represents the mass fraction of particles (mass per unit mass of the gas-particles mixture) of the  $j$ -th family with diameter between  $\phi$  and  $\phi + d\phi$ . Again, the shape of the distribution  $\gamma_j(\phi)$  can be characterized by its moments  $\Pi_j^i$ , defined by

$$\Pi_j^{(i)} = \int_{-\infty}^{+\infty} \phi^i \gamma_j(\phi) d\phi. \quad (10)$$

175 Also in this case the particular definition of  $\gamma_j(\phi)$  allows a physical interpretation of the moments:  
 for example, the moment  $\Pi_j^{(0)}$  is the mass fraction of the  $j$ -th solid phase  $x_{s,j}$  with respect to  
 the gas-particles mixture. As done with the particle number distribution, it is possible to define a  
 mean particle size in terms of the moments of the mass fraction distribution as  $\Pi_j^{(i+1)}/\Pi_j^{(i)}$ ; this  
 ratio, for  $i = 0$ , gives the mass averaged diameter, corresponding to the volume averaged diameter  
 180  $L_{j,43} = M_j^{(4)}/M_j^{(3)}$  when the density  $\rho_{s,j}(\phi)$  is constant.

Again, it is possible to define the moments of other quantities  $\psi_j(\phi)$  in terms of the continuous  
 distribution of mass fraction  $\gamma_j(\phi)$  as

$$\psi_j^{(i)} = \frac{1}{\Pi_j^{(i)}} \int_{-\infty}^{+\infty} \psi_j(\phi) \phi^i \gamma_j(\phi) d\phi. \quad (11)$$

For example, when the mass fraction distribution  $\gamma_j(\phi)$  is used, the mass averaged heat capacity  
 185  $\bar{C}_{s,j}$  is given by the following expression:

$$\bar{C}_{s,j} = \frac{1}{x_{s,j}} \int_{-\infty}^{+\infty} C_{s,j}(\phi) \gamma_{s,j}(\phi) d\phi = C_{s,j}^{(0)} \quad (12)$$

and the volumetric averaged density, i.e. the mass of particles per unit volume, can be evaluated from

$$\bar{\rho}_{s,j} = \frac{1}{x_{s,j}} \int_{-\infty}^{+\infty} \frac{\gamma_{s,j}(\phi)}{\rho_{s,j}(\phi)} d\phi = \left[ \frac{1}{\rho_{s,j}} \right]^{(0)}. \quad (13)$$

### 190 3 Plume Model

In this section we describe the assumption and the equations of the model. As in Bursik (2001), the  
 model assumes an homogeneous mixture of particles and gases with thermal and mechanical equi-  
 librium between all phases. Aggregation and breakage effects are not considered and consequently  
 density does not change with time. Finally, the model does not consider effects of humidity and  
 195 water phase changes.

The equation set for the plume rise model is solved in a 3-D coordinate system  $(s, \eta, \theta)$  by consid-  
 ering the bulk properties of the eruptive mixture (see Figure 1). The plume is assumed with a circular  
 section in the plane normal to the centerline trajectory with curvilinear coordinate  $s$ , a top-hat pro-  
 file of the velocity along the centerline, an inclination on the ground defined by an angle  $\eta$  between  
 200 the axial direction and the horizon, and an angle  $\theta$  in the horizontal plane  $(x, y)$  with respect to the  
 $x$ -axis. These angles are needed to describe the evolution of weak explosive eruptions which are  
 strongly affected by atmospheric conditions.

Following Bursik et al. (1992) and Ernst et al. (1996), the conservation of flux of particles with  
 size  $D$  of the  $j$ -th family is given by:

$$205 \frac{d}{ds} (f_j(D) \pi r^2 U_{sc}) = -2\pi r p w_{s,j}(D) f_j(D) \quad (14)$$

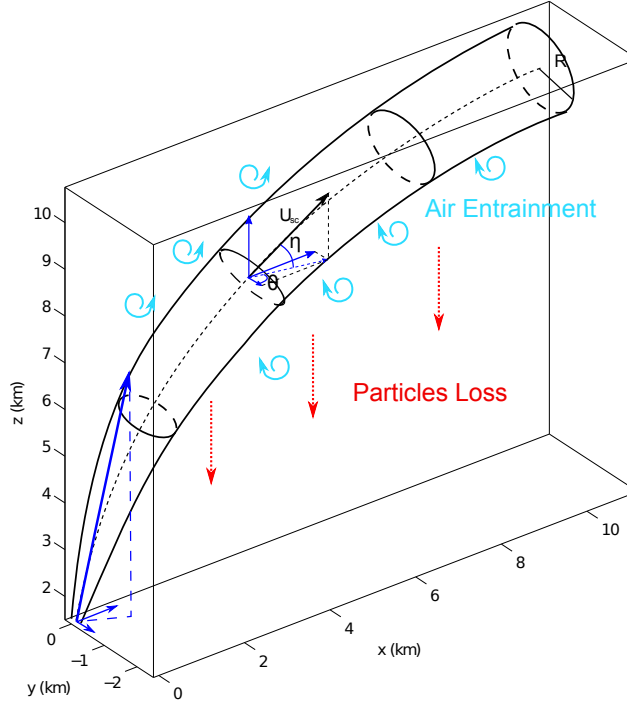


**Figure 1.** Schematic representation of the Eulerian plume model. The dashed black line represent the axis of the curvilinear coordinate  $s$ .

where  $r$  is characteristic plume radius,  $U_{sc}$  represents the velocity of the plume cross section along its centerline (a top-hat profile is assumed) and  $p$  is the probability that an individual particle will fall out of the plume, defined as a function of an entrainment coefficient  $\alpha$  as

$$p = \frac{\left(1 + \frac{6}{5}\alpha\right)^2 - 1}{\left(1 + \frac{6}{5}\alpha\right)^2 + 1}. \quad (15)$$

210 Equation (14) states that the number of particles of the  $j$ -th family with size  $D$  lost from the plume is proportional to the number of particles at the plume margin, given by  $f_j(D) \cdot 2\pi r$ , to the settling velocity  $w_{s,j}(D)$  and to the probability factor  $p$ .

Now, multiplying both the sides of equation (14) for  $D^i$  and then integrating over the size spectrum  $[0, +\infty]$ , we obtain the following conservation equations for the moments  $M_j^{(i)}$ :

$$215 \quad \frac{d}{ds} \left( M_j^{(i)} U_{sc} r^2 \right) = -2rpw_{s,j}^{(i)} M_j^{(i)}. \quad (16)$$

If we compare our formulation with that presented in Barsotti et al. (2008), where the effects of a polydisperse solid phase are taken into account partitioning the size spectrum in a finite number  $N$  of solid classes, the set of equations (16) replaces the  $N$  mass conservation equations for the  $N$  particulate classes.

220 From equation (14), if we multiply both the terms by the mass of the particles of size  $D$ , given by  $\frac{\pi}{6}D^3\rho_{s,j}(D)$ , we obtain the additional equation:

$$\begin{aligned} \frac{d}{ds} \left( f_j(D) \frac{\pi}{6} D^3 \rho_{s,j}(D) \pi r^2 U_{sc} \right) = \\ -2\pi r p w_{s,j}(D) f_j(D) \frac{\pi}{6} D^3 \rho_{s,j}(D) \end{aligned} \quad (17)$$

and, integrating over the size spectrum:

$$\frac{d}{ds} \left( U_{sc} r^2 \frac{\pi}{6} M_j^{(3)} \rho_{s,j}^{(3)} \right) = -2r p \frac{\pi}{6} M^{(3)} [w_{s,j} \rho_{s,j}]^{(3)}, \quad (18)$$

225 where on the left hand-side the term  $\frac{\pi}{6} M_j^{(3)} \rho_{s,j}^{(3)}$  represents the volume average bulk density of the particles of the  $j$ -th family (i.e. the mass of particles of the  $j$ -th family per unit volume of gas-particles mixture, denoted with the superscript  $B$ ,  $\rho_{s,j}^B$ ), while on the right-hand side the term  $[w_{s,j} \rho_{s,j}]^{(3)}$  represents the mass averaged settling velocity of the particles of the  $j$ -th family multiplied by the volume averaged particles density. Equation (18) is the mass conservation equation for the  $j$ -th  
230 family of particles, relating the variation of the mass flux of particles within the plume with the loss at the plume margin.

Now, following the same procedure, we reformulate the other conservation equations describing the steady-state ascent of the plume in terms of the moments of the continuous distributions of sizes, densities and settling velocities instead of the averages over a finite number of classes of particles  
235 with different size.

First of all, we derive the conservation equation for the mixture mass. As in the plume theory, we assume that the entrainment, due to both turbulence in the rising buoyant jet and to the cross-wind field, is parameterized through the use of two entrainment coefficients,  $\alpha_\epsilon$  and  $\gamma_\epsilon$ . The theory assumes that the efficiency of mixing with ambient air is proportional to the product of a reference  
240 velocity (the vertical plume velocity in one case and the wind field component along the plume centerline in the other), by  $\alpha_\epsilon$  and  $\gamma_\epsilon$  (Morton, 1959; Briggs, 1975; Wright, 1984; Weil, 1988). Thus, following Hewett et al. (1971) and Bursik (2001), we define the entrainment velocity  $U_\epsilon$  as a function of windspeed,  $U_{atm}$ , as well as axial plume speed,  $U_{sc}$ :

$$U_\epsilon = \alpha_\epsilon |U_{sc} - U_{atm} \cos \phi| + \gamma_\epsilon |U_{atm} \sin \phi| \quad (19)$$

245 where  $\alpha_\epsilon |U_{sc} - U_{atm} \cos \phi|$  is entrainment by radial inflow minus the amount swept tangentially along the plume margin by the wind, and  $\gamma_\epsilon |U_{atm} \sin \phi|$  is entrainment from wind. With this notation, the total mass conservation equation solved by the model becomes

$$\frac{d}{ds} (\rho_{mix} U_{sc} r^2) = 2r \rho_{atm} U_\epsilon - 2r p \sum_j \frac{\pi}{6} M_j^{(3)} [w_{s,j} \rho_{s,j}]^{(3)}, \quad (20)$$

stating that the variation of mass flux (left-hand side term) is due to air entrainment (first right-hand  
250 side term) and loss of solid particles (second right-hand side term), as obtained from Eq. (18).



From Newton's second law and the variation of mass flux, we can derive also the horizontal and vertical components of the momentum balance solved by the model as:

$$\begin{aligned} \frac{d}{ds} (\rho_{mix} U_{sc} r^2 (u - U_{atm})) = \\ -r^2 \rho_{mix} w \frac{dU_{atm}}{dz} - 2upr \sum_j \frac{\pi}{6} M_j^{(3)} [w_{s,j} \rho_{s,j}]^{(3)}, \end{aligned} \quad (21)$$

and

$$\begin{aligned} \frac{d}{ds} (\rho_{mix} U_{sc} r^2 w) = \\ gr^2 (\rho_{atm} - \rho_{mix}) - 2wpr \sum_j \frac{\pi}{6} M_j^{(3)} [w_{s,j} \rho_{s,j}]^{(3)}, \end{aligned} \quad (22)$$

255

where the two components of plume velocity along the horizontal and vertical axes are  $u$  and  $w$ , respectively, and they are linked by the relation  $U_{sc} = \sqrt{u^2 + w^2}$ . In the right-hand side of equation (21) the terms related to the exchange of momentum due to the wind (Barsotti et al., 2008) and to momentum loss from the fall of solid particles appear. Similar contributions are evident in the right-hand side term of equation (22) where the vertical momentum is changed by the gravitational acceleration term and the fall-out of particles.

260

Now, following the notation adopted above and denoting with  $T$  the mixture temperature, the equation for conservation of thermal energy solved by the model writes as

$$\begin{aligned} \frac{d}{ds} (\rho_{mix} U_{sc} r^2 C_{mix} T) = 2r \rho_{atm} U_{sc} C_{atm} T_{atm} \\ -r^2 w \rho_{atm} g - 2Tpr \sum_j \frac{\pi}{6} M_j^{(3)} [C_{s,j} w_{s,j} \rho_{s,j}]^{(3)}. \end{aligned} \quad (23)$$

265

The first term on right-hand side describes the cooling of the plume due to ambient air entrainment, the second one takes into account atmospheric thermal stratification, and the third term allows for heat loss due to loss of solid particles. Again, this last term is obtained writing the heat loss for the particles of size  $D$ , and then integrating over the size spectrum. A thermal equilibrium between solid and gaseous phases is assumed. In Eq. (23)  $C_{atm}$  and  $C_{mix}$  are the heat capacity of the entrained atmospheric air and of the mixture, respectively, the latter being defined as:

270

$$C_{mix} = (1 - \sum_j x_{s,j}) C_{p,g} + \sum_j x_{s,j} \bar{C}_{s,j} \quad (24)$$

or, in terms of the bulk densities  $\rho_{atm}^B = x_{atm} \rho_{mix}$ ,  $\rho_{wv}^B = x_{wv} \rho_{mix}$  and  $\rho_{s,j}^B = \frac{\pi}{6} M_j^{(3)} \tilde{\rho}_{s,j}$ , as

$$C_{mix} = \frac{\rho_{atm}^B C_{atm} + \rho_{wv}^B C_{wv} + \sum_j \rho_{s,j}^B \bar{C}_{s,j}}{\rho_{atm}^B + \rho_{wv}^B + \sum_j \rho_{s,j}^B}. \quad (25)$$

From this expression, if we multiply all the terms at the numerator and the denominator of the right-hand side by  $U_{sc}r^2$  and we differentiate with respect to  $s$ , we obtain after some cancellation and algebra manipulations the following equation for the variation of the mixture specific heat with  $s$ :

$$\begin{aligned} \frac{dC_{mix}}{ds} = & \\ & \frac{1}{\rho_{mix}U_{sc}r^2} \left[ (C_{atm} - C_{mix}) \frac{d}{ds} (\rho_{atm}^B U_{sc}r^2) \right. \\ & \left. + \sum_j (\bar{C}_{s,j} - C_{mix}) \frac{d}{ds} (\rho_{s,j}^B U_{sc}r^2) \right] \\ & + \sum_j \frac{\rho_{s,j}^B}{\rho_{mix}} \left[ \frac{\frac{d}{ds} (\bar{C}_{s,j} \rho_{s,j}^B U_{sc}r^2)}{\rho_{s,j}^B U_{sc}r^2} - \frac{\bar{C}_{s,j} \frac{d}{ds} (\rho_{s,j}^B U_{sc}r^2)}{\rho_{s,j}^B U_{sc}r^2} \right]. \end{aligned} \quad (26)$$

Now, substituting the expressions for the derivatives appearing in each term on the right-hand side, we obtain the equation for the variation rate of mixture specific heat in terms of the moments:

$$\begin{aligned} \frac{dC_{mix}}{ds} = & \frac{1}{\rho_{mix}U_{sc}r^2} \left[ C_{atm} 2r \rho_{atm} U_\epsilon - C_{mix} \left( 2r \rho_{atm} U_\epsilon \right. \right. \\ 280 \quad & \left. \left. - 2pr \sum_j \frac{\pi}{6} M_j^{(3)} [w_{s,j} \rho_{s,j}]^{(3)} \right) \right. \\ & \left. - 2pr \sum_j \frac{\pi}{6} M_j^{(3)} [w_{s,j} \rho_{s,j} C_{s,j}]^{(3)} \right] \end{aligned} \quad (27)$$

Similarly, a gas constant  $R_g$  can be defined as a weighted average of the gas constant for the entrained atmospheric air  $R_{atm}$  and the gas constant of the volcanic water vapour  $R_{wv}$

$$R_g = \frac{\rho_{atm}^B R_{atm} + \rho_{wv}^B R_{wv}}{\rho_{atm}^B + \rho_{wv}^B} \quad (28)$$

and a conservation equation can be derived, knowing that the variation of gaseous mass fraction with height is solely due to entrained air:

$$\frac{dR_g}{ds} = \frac{R_{atm} - R_g}{\rho_{mix}(1 - x_s)U_{sc}r^2} \cdot 2r \rho_{atm} U_\epsilon. \quad (29)$$

This formulation reduces, for particular cases, to the expressions of Woods (1988) and Glaze and Baloga (1996). Equations (27) and (29) are needed in order to close the system of equations and recover the new values of the temperature and the mixture density once the system of ordinary differential equations is integrated. Otherwise, without the solutions of Equations (27) and (29), we should use the old values of  $\rho_{mix}$  and  $C_{mix}$  at  $s$  to obtain the values of the temperature at  $s + ds$  from the lumped term  $(\rho_{mix}U_{sc}r^2 C_{mix}T)$  obtained integrating Eq. (23).

Finally, as in Bursik (2001), the equations expressing the coordinate transformation between  $(x, y, z)$  and  $(s, \eta, \theta)$  are given by:

$$295 \quad \frac{dz}{ds} = \sin \eta, \quad \frac{dx}{ds} = \cos \eta \cos \theta, \quad \frac{dy}{ds} = \cos \eta \sin \theta. \quad (30)$$

### 3.1 Mass fraction distribution

Similarly as done for the distribution of particle number  $f_j(D)$  and the moments  $M_j^{(i)}$ , it is possible to derive a set of conservation equations in terms of the moments  $\Pi_j^{(i)}$  of the mass fraction distribution  $\gamma_j(\phi)$  expressed as a function of the Krumbein scale.

300 In this case, the conservation of mass flux of particles with size  $\phi$  of the  $j$ -th family write as:

$$\frac{d}{ds} (\rho_{mix} \gamma_j(\phi) \pi r^2 U_{sc}) = -2\pi r p w_{s,j}(\phi) \rho_{mix} \gamma_j(\phi). \quad (31)$$

Multiplying both sides of the equation by  $\phi^i$  and integrating over the size spectrum  $[-\infty, +\infty]$ , we obtain the following conservation equations for the moments of the continuous distributions  $\gamma_j(\phi)$ :

$$\frac{d}{ds} (\Pi_j^{(i)} \rho_{mix} U_{sc} r^2) = -2r p \rho_{mix} w_{s,j}^{(i)} \Pi_j^{(i)}. \quad (32)$$

305 For  $i = 0$ , the equations of conservation of the moments give:

$$\frac{d}{ds} (x_{s,j} \rho_{mix} U_{sc} r^2) = -2r p \rho_{mix} w_{s,j}^{(0)} x_{s,j} \quad (33)$$

expressing the loss of mass flux of the particles of the  $j$ -th family and thus we can write the total mass conservation equation as

$$\frac{d}{ds} (\rho_{mix} U_{sc} r^2) = 2r \rho_{atm} U_\epsilon - 2r p \rho_{mix} \sum_j w_{s,j}^{(0)} \Pi_j^{(0)}. \quad (34)$$

310 From the variation of mass flux, as done for the distribution of particle number  $f_j(D)$  and the moments  $M_j^{(i)}$ , we derive the horizontal and vertical components of the momentum balance:

$$\frac{d}{ds} (\rho_{mix} U_{sc} r^2 (u - U_{atm})) = -r^2 \rho_{mix} w \frac{dU_{atm}}{dz} - 2upr \rho_{mix} \sum_j w_{s,j}^{(0)} \Pi_j^{(0)}, \quad (35)$$

$$\frac{d}{ds} (\rho_{mix} U_{sc} r^2 w) = gr^2 (\rho_{atm} - \rho_{mix}) - 2wpr \rho_{mix} \sum_j w_{s,j}^{(0)} \Pi_j^{(0)}. \quad (36)$$

315 The equation for conservation of thermal energy is

$$\frac{d}{ds} (\rho_{mix} U_{sc} r^2 C_{mix} T) = 2r \rho_{atm} U_\epsilon C_{atm} T_{atm} - r^2 w \rho_{atm} g - 2Tpr \rho_{mix} \sum_j [C_{s,j} w_{s,j}]^{(0)} \Pi_j^{(0)} \quad (37)$$

and the equation for the variation rate of mixture specific heat in terms of the moments of the mass fraction distribution write as:

$$\begin{aligned} \frac{\partial C_{mix}}{\partial s} = \frac{1}{\rho_{mix} U_{sc} r^2} & \left[ C_{atm} 2r \rho_{atm} U_\epsilon - C_{mix} (2r \rho_{atm} U_\epsilon \right. \\ & \left. - 2r p \rho_{mix} \sum_j w_{s,j}^{(0)} \Pi_j^{(0)}) - 2p r \rho_{mix} \sum_j [C_{s,j} w_{s,j}]^{(0)} \Pi_j^{(0)} \right]. \end{aligned} \quad (38)$$

320 The formulation of the equations for the gas constant  $R_g$  and the coordinates of the  $(x, y, z)$  remain unchanged.

#### 4 Numerical scheme

The plume rise equations are solved with a predictor-corrector Heun's scheme (Petzold and Ascher, 1998) that guarantees a second-order accuracy, keeping the execution time in the order of seconds.

325 If we rewrite the system of ordinary differential equations with the following compact notation:

$$\frac{dy}{ds} = f(s, y), \quad y(s_0) = y_0, \quad (39)$$

where  $y$  is the vector of the quantities in the left-hand sides of the conservation equations presented in the previous section, then the procedure for calculating the numerical solution by way of Heun's method (Süli and Mayers, 2003) is to first calculate the intermediate values  $\tilde{y}_{i+1}$  and then the solution

330  $y_{i+1}$  at the next integration point

$$\begin{aligned} \tilde{y}_{i+1} &= y_i + ds f(s_i, y_i), \quad \text{predictor step} \\ y_{i+1} &= y_i + \frac{ds}{2} (f(s_i, y_i) + f(s_{i+1}, \tilde{y}_{i+1})) \quad \text{corrector step.} \end{aligned} \quad (40)$$

##### 4.1 Quadrature method of moments

We observe that to calculate the right-hand side for both the predictor and corrector step we need not only the moments  $M^{(i)}$ , but also the additional moments  $[w_s]^i$ ,  $[w_s \rho_s]^{(i)}$  and  $[w_s \rho_s C_s]^{(i)}$ . As in

335 Marchisio and Fox (2013), the integral in the definition of these moments is replaced by a quadrature formula and the moments, for a generic variable  $\psi = \psi(D)$ , are approximated as:

$$\psi^{(i)} = \frac{1}{M^{(i)}} \int_0^{+\infty} \psi(D) f(D) D^i dD \approx \sum_{l=1}^N \psi(D_l) D_l^i \omega_l \quad (41)$$

Here  $\omega_l$  and  $D_l$  are known as “weights” and “nodes” (or “abscissae”) of the quadrature, respectively, and the accuracy of a quadrature formula is quantified by its degree. The degree of accuracy

340 is equal to  $d$  if the interpolation formula is exact when the integrand is a polynomial of order less

than or equal to  $d$  and there exists at least one polynomial of order  $d + 1$  that makes the interpolation formula inexact. In particular, an  $N$ -point Gaussian quadrature rule, is a quadrature rule constructed to yield an exact result for polynomials of degree  $2N - 1$  or less by a suitable choice of the nodes  $D_l$  and weights  $\omega_l$  for  $l = 1, \dots, N$  (Golub and Welsch, 1969).

345 The Wheeler algorithm, as presented in Marchisio and Fox (2013), provides an efficient  $O(N^2)$  algorithm for finding a full set of weights and abscissas for a realizable moment set. The resulting nodes  $D_l$  are always within the support (and therefore represent realizable values of the particle size), and the weights  $\omega_l$  are always positive, ensuring that, when the quadrature is used, accurate results are obtained Marchisio and Fox (2013). Nevertheless, these properties are respected only if  
 350 the moment set is realizable, meaning that there exists a particle size distribution resulting in that specific set of moments.

A strategy that might overcome the problem of moment corruption (i.e. the transformation during the integration of the moment-transport equations of a realizable set of moments into an unrealizable one) is replacing unrealizable moment sets as soon as they appear. An algorithm of this kind was  
 355 developed by McGraw (McGraw, 2006). The algorithm first verifies whether the moment set is realizable (by looking at the second-order difference vector or by looking at the Hankel-Hadamard determinants (Gautschi, 2004)). If the moment set is unrealizable it proceeds with the correction. In the numerical model here presented, the implementation of the correction algorithm of Wright is derived from the version presented in Marchisio and Fox (2013).

360 Thus, in both the predictor and corrector step, the following algorithm is used:

- the nodes  $D_{j,l}$  and weights  $\omega_{j,l}$  are calculated with the Wheeler algorithm for  $l = 1, \dots, N$ ;
- the quadrature formula (41) is used to evaluate the moments  $[w_s]_j^{(i)}$ ,  $[w_s \rho_s]_j^{(i)}$  and  $[w_s \rho_s C_s]_j^{(i)}$ ;
- the right-hand side of the ODE's system (39) is evaluated explicitly;
- the solution is advanced with the predictor (or the corrector) step of the Heun's scheme;
- 365 – for each particle family  $j$ , the moments  $M_j^{(i)}$  ( $i = 0, \dots, 2N - 1$ ), if required, are corrected with the McGraw (or Wright) algorithm.

We observe that if the  $j$ -th family of particles is monodisperse with diameter  $\bar{d}_j$ , the Wheeler algorithm fed with the first two moments only gives as result a single quadrature node  $D_{j,1} = \bar{d}_j$  with weight  $\omega_{j,1} = 1$ . This allows us also to use the model for the simplified case where the solid  
 370 particle distribution is partitioned in a finite number of classes with constant size, assigning to each class a monodisperse distribution.

## 4.2 Initial condition

Initial conditions at the vent include the initial plume radius ( $r_0$ ), mixture velocity ( $U_{sc,0}$ ) and temperature ( $T_0$ ), gas mass fraction ( $n_0$ ) and the particles size distribution through the initial moments

375  $M_0^{(i)}$ . In the next section we derive analytically the moments of a specific initial distribution (a normal distribution in the Krumbein scale) for both the formulations based on the number of particles as a function of the particles diameter expressed in meters and the formulation based on the mass concentration expressed as a function of the phi scale.

#### 4.2.1 Lognormal distribution

380 For the application presented in this work, the initial distribution  $f(D)$  at the base of the plume is defined as a function of the particles diameter expressed in meters ( $m$ ), in order to give a corresponding normal distribution with parameters  $\mu$  and  $\sigma$  for the mass concentration expressed as a function of the Krumbein phi ( $\phi$ ) scale (when all the particles have the same density):

$$\gamma(\phi) = \frac{K_0}{\sigma\sqrt{2\pi}} e^{-\frac{(\phi-\mu)^2}{2\sigma^2}}, \quad (42)$$

385 where  $K_0$  is a parameter that has to be chosen in order to satisfy the initial condition on the solid mass fraction.

Given the parameters  $\mu$  and  $\sigma$ , the initial distribution  $f(D)$  is then written as:

$$f(D) = \frac{6C_0}{(-\sigma \ln 2) D^4 \sqrt{2\pi^3}} e^{-\frac{[-\ln(1000D) - \mu \ln 2]^2}{2(\sigma \ln 2)^2}}. \quad (43)$$

390 where  $C_0$ , analogously to  $K_0$ , is a parameter that has to be fixed in order to satisfy the initial condition prescribed for the mass (or volume) fraction of particles.

We observe that if we introduce the following re-scaled variables for the diameter, the mean and the variance:

$$\bar{D} = 1000D, \quad \bar{\mu} = -\mu \ln 2, \quad \bar{\sigma} = -\sigma \ln 2, \quad (44)$$

395 then it is possible to rewrite the particle distribution  $f(D)$  in terms of a lognormal distribution in the variable  $\bar{D}$  with parameters  $\bar{\mu}$  and  $\bar{\sigma}$ :

$$\begin{aligned} \bar{f}(\bar{D}) &= \frac{6 \cdot 10^{12} C_0}{\pi \bar{D}^3} \frac{1}{\bar{\sigma} \bar{D} \sqrt{2\pi}} e^{-\frac{[\ln(\bar{D}) - \bar{\mu}]^2}{2\bar{\sigma}^2}} \\ &= \frac{6 \cdot 10^{12} C_0}{\pi \bar{D}^3} \text{lognorm}(\bar{D}, \bar{\mu}, \bar{\sigma}). \end{aligned} \quad (45)$$

Consequently, we can evaluate the moments  $M^{(i)}$  of  $f(D)$  analytically from the moments of the lognormal distribution as:

$$M^{(i)} = \frac{6C_0}{\pi} 10^{3(3-i)} \exp \left[ (i-3)\bar{\mu} + \frac{1}{2}(i-3)^2 \bar{\sigma}^2 \right], \quad (46)$$

400 and we obtain, for the third moment:

$$M^{(3)} = \frac{6C_0}{\pi} \Rightarrow C_0 = \alpha_s^0 \quad (47)$$

where  $\alpha_s^0$  is the initial volume fraction of the particles in the solid-gas mixture.

From the expressions of the moments it follows also that, if the mass concentration expressed as a function of the Krumbein scale has a normal distribution, the Sauter mean diameter  $D_A$  expressed  
 405 in meters can be evaluated as

$$D_A = L_{32} = \frac{M^{(3)}}{M^{(2)}} = 10^{-3} \exp\left(\bar{\mu} - \frac{1}{2}\bar{\sigma}^2\right), \quad (48)$$

or, if expressed in  $\phi$ , as

$$D_A^\phi = L_{32}^\phi = \mu + \frac{1}{2}\sigma^2 \ln(2). \quad (49)$$

Processes involving the mutual interaction between particles and the interaction between the par-  
 410 ticles and the carrier fluid (friction and cohesion between the particles; viscous drag; chemical reac-  
 tions between fluid and solid components) operate at the surface of the particles. For this reason the  
 Sauter mean diameter, based on the specific area of the particles, is a convenient descriptor and it is  
 important to remark that it differs from the mean  $\mu$  of the lognormal distribution by a factor propor-  
 tional to the variance  $\sigma^2$ . For numerical models describing the multiphase (particulate) nature of the  
 415 matter and which approximate the particle size distribution with an average size, it is hence more ap-  
 propriate to use, as particle size representative of a lognormal distribution, the Sauter mean diameter  
 than the mean diameter  $\mu$ . The difference between the two approximations is smaller the narrower  
 the particle size distribution. We must also remark that, while for particles in the inertial-dominated  
 regime (e.g.  $Re_p > 2000$ ) Loth et al. (2004) showed that the Sauter mean diameter is the effective  
 420 diameter, regardless of particle shape, particle size distribution, particle density distribution or net  
 volume fraction, for particles in the creeping flow regime ( $Re_p \ll 1$ ) the effective mean diameter  
 is the volume-width diameter.

When the Sauter mean diameter is used, also the variance and the standard deviation SD should  
 be based on the specific surface area (Rietema, 1991). Hence:

$$425 \sigma_A^2 = \int_0^{+\infty} \left(\frac{1}{D} - \frac{1}{D_A}\right)^2 \frac{\pi}{6} D^3 f(D) dD, \quad (50)$$

or, expressed as a function of the moments:

$$\sigma_A^2 = \frac{M^{(1)}M^{(3)} - (M^{(2)})^2}{(M^{(3)})^2}. \quad (51)$$

Finally, we note that if the particle density is constant and the mass concentration expressed as  
 a function of the Krumbein scale has a lognormal distribution and both the Sauter mean diameter  
 430  $L_{32} = M^{(3)}/M^{(2)}$  and the mean particle length averaged with respect to particle number density  
 $L_{10} = M^{(1)}/M^{(0)}$  (or if the first 4 moments) are known then we can solve for the re-scaled mean  
 and variance  $\bar{\mu}$  and  $\bar{\sigma}$  the following system:

$$\begin{cases} L_{10} = 10^{-3} \exp\left(\bar{\mu} - \frac{5}{2}\bar{\sigma}^2\right) \\ L_{32} = 10^{-3} \exp\left(\bar{\mu} - \frac{1}{2}\bar{\sigma}^2\right) \end{cases}. \quad (52)$$

Once the re-scaled mean and variance are known, we can obtain  $\mu$  and  $\sigma$  in the Krumbein  $\phi$  scale.

435 When the initial distribution is expressed for the mass fractions instead of the particle number, and the mass fraction written as a function of the Krumbein scale has a normal distribution with mean  $\mu$  and variance  $\sigma^2$ , then the continuous distribution is given by Eq. (42). We observe that this expression of the distribution is not based on the assumption of constant density for the particles of different size.

440 In this case, the moments  $\Pi^{(i)}$  are given by the following expression

$$\Pi^{(i)} = K_0 \sum_{j=0}^{\lceil i/2 \rceil} \binom{i}{2j} (2j-1)!! \sigma^{2j} \mu^{i-2j}. \quad (53)$$

where the symbols  $\lceil \cdot \rceil$  and  $!!$  denote the integer part and the double factorial ( $n!! = \prod_{k=0}^m (n-2k)$ , where  $m = \lceil n/2 \rceil - 1$ ), respectively.

Now, as the 0-th moment is equal to the mass fraction of particles, we obtain  $K_0 = x_s$ . Furthermore, we observe that the mass fraction averaged diameter in the  $\phi$  scale is given by the ratio  $\Pi^{(1)}/\Pi^{(0)}$ , while the variance of the mass fraction distribution can be evaluated as  $[\Pi^{(2)}\Pi^{(0)} - (\Pi^{(1)})^2]/(\Pi^{(0)})^2$ . These two quantities correspond to the parameters  $(\mu, \sigma^2)$  generally used to describe the mass fraction when a normal distribution in the  $\phi$  scale is assumed. For this reason, when we want to track the changes of the mass fraction averaged diameter and its standard deviation (or variance) in the  $\phi$  scale during the plume rise, it is preferred to use a formulation based on the moments  $\Pi^{(i)}$  than the moments  $M^{(i)}$ .

445  
450

## 5 Application

### 5.1 Simulation inputs

We applied the model to three different test cases with different vent and atmospheric conditions:

- 455
- Test Case 1 - low-flux plume without wind;
  - Test Case 2 - low-flux plume with wind (weak bent plume);
  - Test Case 3 - high-flux plume (strong plume).

The parameters used for the different test cases are listed in Table 1, while the atmospheric conditions are plotted in Fig. 3. For the low-flux plumes a mass flow rate of  $1.5 \times 10^6$  kg/s has been fixed, while for the strong plume the value is  $1.5 \times 10^9$  kg/s. The temperature pressure and density profiles used for the test case without wind (Test Case 1) are those defined by the International Organization for Standardization for the International Standard Atmosphere (Champion et al., 1985), while the profiles for the other two test cases come from reanalysis data.

460



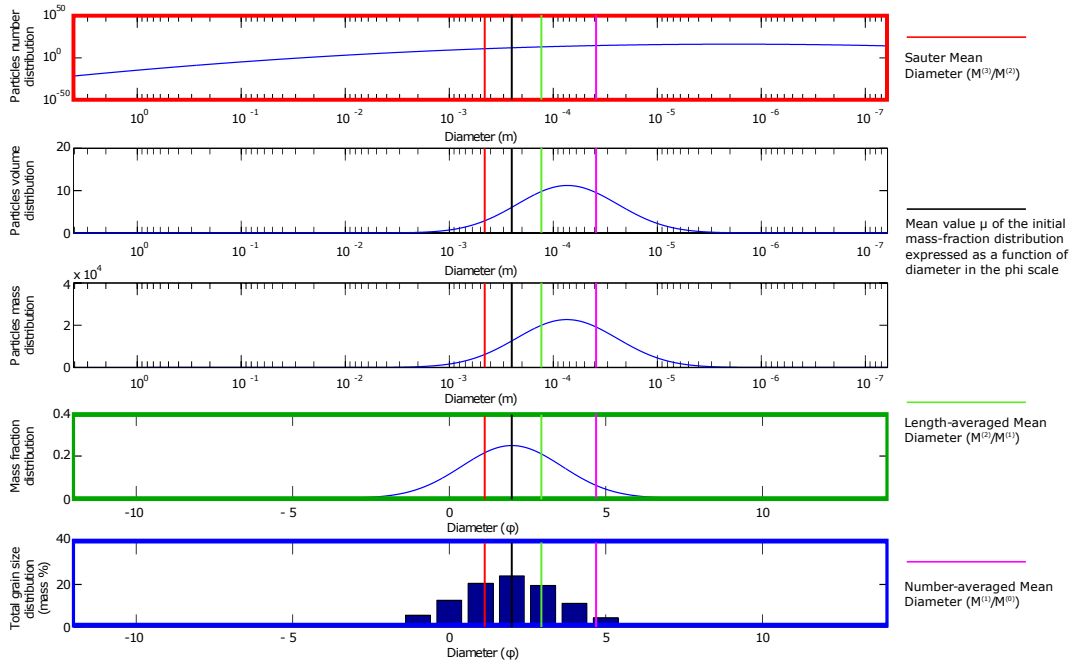


**Figure 2.** Visualization of a normal initial distribution in the Krumbein  $\phi$  scale for the solid particles. On the top the particle number distribution expressed as a function of the diameter expressed in meters is plotted. On the second and third plots from the top the corresponding distributions of volume and mass are plotted, these two being different because the density is a function of the diameter. On the fourth plot the continuous distribution (lognormal) of mass fraction as a function of the  $\phi$  scale is plotted, while in the last plot the distribution has been discretized with 13 bins in the range  $(-4;8)$ . On each panel different average radii are also plotted, together with the mean of the initial distribution. The first, fourth and fifth panel are highlighted with different color, also used in Fig. 4 for the solutions obtained with the three different representation of the initial grain size distribution.

For all the runs presented here, a single family of particles has been used, with a normal distribution (with parameters  $\mu$  and  $\sigma$ ) for the mass concentration as a function of the diameter expressed in the  $\phi$  scale and with density varying with the particle diameter.

We first present a comparison of the plume profiles obtained with the 3 different descriptions presented in the previous sections and highlighted in the three colored boxes of Fig. 2 for the Test Case 2: method of moments for the particle number being function of the size expressed in meters; method of moments for the particle mass fraction being function of the size expressed in the  $\phi$  scale; discretization in uniform bins in the  $\phi$  scale. For this comparison, the mass flow rate at the vent is  $1.5 \times 10^6$  kg/s and a rotating wind is present, as shown in Fig. 3, while the mean and the standard deviation of the initial total grain size distribution are respectively 2 and 1.5, expressed in the  $\phi$  scale. The results of the numerical simulations obtained with the three different formulations are presented in Fig. 4 and they perfectly match, showing that the method of moments (dotted lines), both applied to the continuous distribution of the particle number (red) or to the mass distribution (green), gives

Parameters	Units	Test Case 1	Test Case 2	Test Case 3
Vent Radius	m	27	27	708
Vent Velocity	m/s	135	135	275
Vent Temperature	K	1273	1273	1053
Vent Gass Mass Fraction		0.03	0.03	0.05
Vent Height	m	1500	1500	1500
$\rho_1$	$kg/m^3$	2000	2000	2000
$\rho_2$	$kg/m^3$	2600	2600	2600
$D_1$	$m$	$8 \times 10^{-6}$	$8 \times 10^{-6}$	$8 \times 10^{-6}$
$D_2$	$m$	$2 \times 10^{-3}$	$2 \times 10^{-3}$	$2 \times 10^{-3}$
$\mu$	$\phi$	-1.0-3.0	-1.0-3.0	-1.0-3.0
$\sigma$	$\phi$	0.5-2.5	0.5-2.5	0.5-2.5

**Table 1.** Input parameters used for the numerical simulations. Vent height is the elevation of the base of the column above sea level. The values  $\rho_{1,2}$  and  $D_{1,2}$  are used to compute the density of the particles as a function of the diameter, according to the formulation of Bonadonna and Phillips (2003). The values reported for  $\mu$  and  $\sigma$  define the range used for the uncertainty quantification and sensitivity analysis.

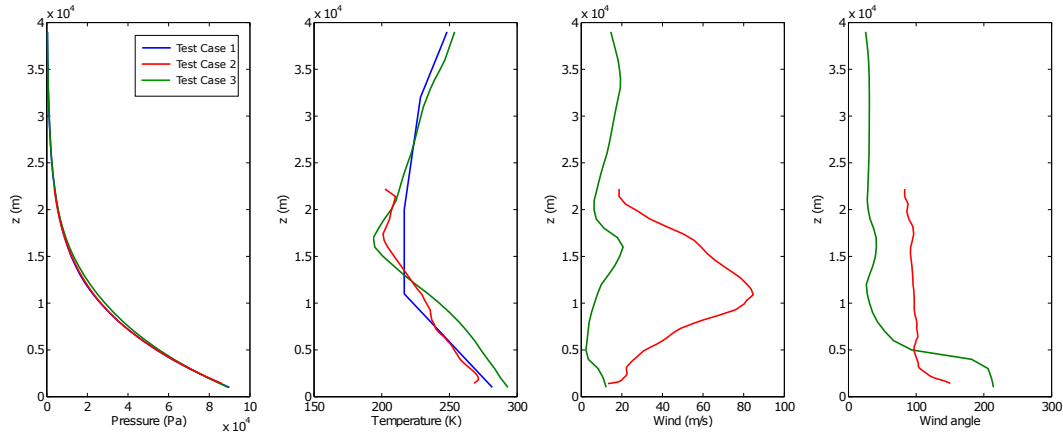


**Figure 3.** Atmospheric profiles for the three test cases. The height is expressed in meters above sea level and for all the test cases the vent is located at 1500m above sea level. For the wind profiles only the profiles for the two test cases with wind are plotted.

the same results of the classical formulation based on the discretization of the mass distribution in bins (solid line). For these simulations, we used only the first 6 moments of the distributions, while 13 bins have been employed with the discretized formulation. This results in a smaller number of equations to solve for the method of moments and, despite the additional cost of the method of moments due to the evaluation of the quadrature points and formulas through the Wheeler algorithm, in a smaller computational time, with a gain of about 30%.

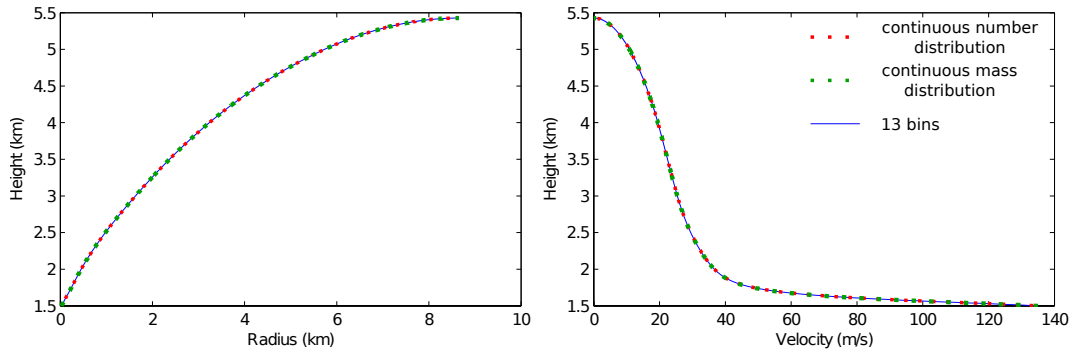


**Figure 4.** Height vs Radius (left) and Velocity (right) for a low-flux plume, simulated with three different models. In blue the profiles obtained using 13 bins, in red the profiles obtained using a continuous distribution of the particle number density and in green using a continuous distribution of the mass fraction.

## 5.2 Simulation results

In this section we want to study the variation during the ascent of solid mass flux (due to particles settling) and of the mean and the variance of the mass distribution along the column. As shown in the previous section, there are no significant differences in the results obtained with the three different descriptions of the grain size distribution. For this reason, in the following we restrict the analysis only to the formulation based on the moments of the mass fraction distribution as a function of the diameter expressed in the  $\phi$  scale. With this approach, the mean, the variance and the skewness of the mass distribution along the column are easily obtained from the first 4 moments  $\Pi^{(i)}$  of the mass fraction distribution.

In Fig. 5 we present the results relative to the Test Case 2 for an initial particle size distribution with mean diameter 2 and standard deviation 1.5, expressed in the  $\phi$  scale. In the left and middle panels the mean, the variance and the skew of the mass fraction distribution are shown respectively, while in the right panel the cumulative loss of solid mass flux is plotted as a percentage of the initial value. We observe a decrease in the mean size of the particles, due to the different settling velocities of particles of different sizes. A decrease in the variance of the size distribution with height is also observed from the second plot. We remark that the particles have a normal distribution only at the base of the column (resulting in a null skewness), and the negative skew at the top of the column indicates that the tail on the left side of the grain size distribution is longer than the tail on the right side, i.e. the mass is more concentrated on the right of the spectrum of particle sizes (finer particles). For this reason we do not have to look at the mean and the variance plotted in Fig. 5 as the parameters of a normal (and symmetric) distribution. Nonetheless changes in the mean, the variance and the skewness are observed, we remark that these changes are quite small and for this reason the parameters of the total grain size distribution at the top of the eruptive column are a good approximation of the parameters at the base of the column, and vice versa. However, this is true

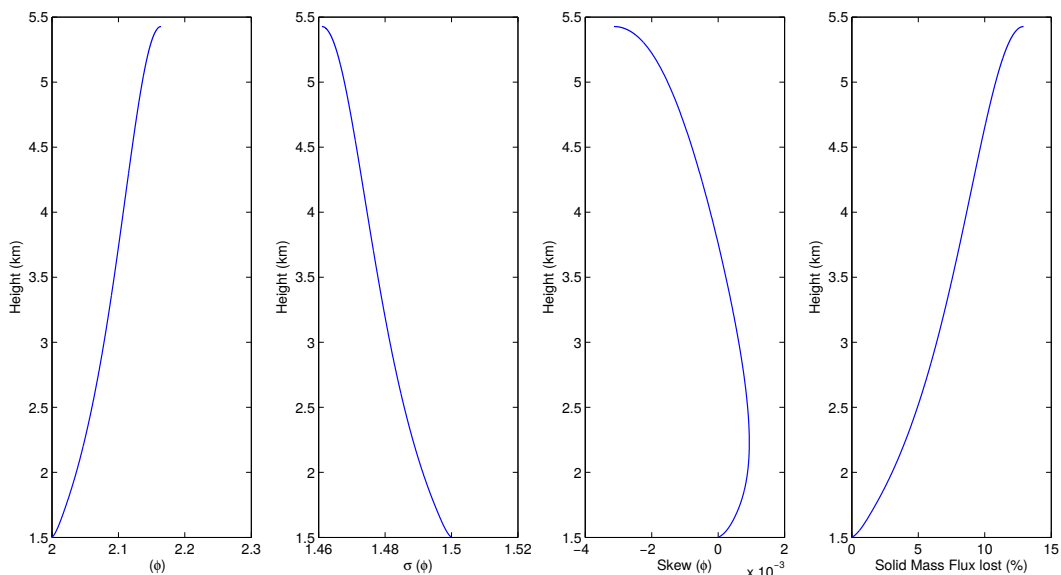


**Figure 5.** Particles distribution parameters (mean, variance and skewness) and cumulative loss of solid mass flux for the test case 2 (low-flux without wind), simulated with the formulation based on the moments of the mass fraction distribution.

for the specific input condition of this test case and not in general. For this reason, it is important to quantify the uncertainty of this assumption for different initial total grain size distributions and different atmospheric conditions.

### 510 5.3 Uncertainty and sensitivity analysis

When dealing with volcanic processes and volcanic hazards, our understanding of the physical system is limited, and vent parameters (volatile contents, temperature, grain size distribution, etc.) are often not well-constrained or are constrained with significant uncertainty. These factors mean that it is difficult to predict the characteristic of the ash cloud released from the volcanic column with  
 515 certainty. An alternative is to quantify the probability of the outcomes (for example the grain size distribution at the top of the column) by coupling deterministic numerical codes with stochastic approaches. It is our goal in this work also to assess the ability to systematically quantify the uncertainty and the sensitivity of the plume model outcomes to uncertain or variable input parameters, in particular to those characterizing the grain size distribution at the base of the eruptive column.

520 Uncertainty quantification (UQ) or nondeterministic analysis is the process of characterizing input uncertainties, propagating forward these uncertainties through a computational model, and performing statistical or interval assessments on the resulting responses. This process determines the effect of uncertainties on model outputs or results. In particular, in this work we wanted to investigate for different test cases the uncertainty in four *response functions* (plume height, solid mass flux lost

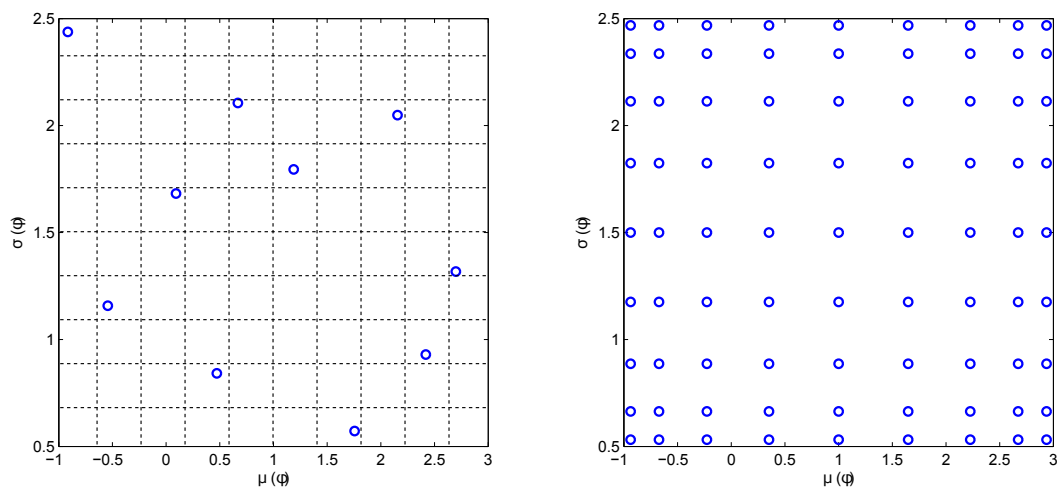


**Figure 6.** Two-parameters Latin Hypercube Sampling with 10 points (left) and tensor product grid using  $9 \times 9$  Clenshaw-Curtis points (right).

525 and mean and variance of the mass fraction distribution at the top of the eruptive column) when the mean and the standard deviation of the distribution at the base are random variables with a uniform probability distribution in the space  $(\mu, \sigma) \in [-1; 3] \times [0.5; 2.5]$ .

In volcanology Monte Carlo simulations are frequently used to perform uncertainty quantification analysis. These methods rely on repeated random sampling of input parameters to obtain numerical  
 530 results; typically one runs simulations many times over in order to obtain the distribution of an unknown output variable. The cost of the Monte Carlo method can be extremely high in terms of number of simulations to run, and thus several alternative approach have been developed. Latin hypercube sampling is another sampling technique for which the range of each uncertain variable is divided into  $N_s$  segments of equal probability, where  $N_s$  is the number of samples requested. The  
 535 relative lengths of the segments are determined by the nature of the specified probability distribution (e.g., uniform has segments of equal width, normal has small segments near the mean and larger segments in the tails). For each of the uncertain variables, a sample is selected randomly from each of these equal probability segments. These  $N_s$  values for each of the individual parameters are then combined in a shuffling operation to create a set of  $N_s$  parameter vectors with a specified correlation  
 540 structure. Compared to Monte Carlo sampling, the Latin hypercube sampling has the advantage that in the resulting sample set every row and column in the hypercube of partitions has exactly one sample, and thus a smaller number of samples is required to cover all the parameter space. In the left panel of Fig. 6 an example of Latin hypercube sampling with  $N_s = 10$  and a uniform distribution probability for both  $\mu$  and  $\sigma$  is plotted.

545 An alternative approach to uncertainty quantification is the so-called generalized Polynomial Chaos Expansion method (gPCE), a technique that mirrors **deterministic finite element analysis**

utilizing the notions of projection, orthogonality, and weak convergence (Ghanem and Red-Horse, 1999). PCE was developed by Norbert Wiener in 1938 and it soon become widely used because of its efficiency when compared to Monte Carlo simulations. The term "Chaos" here simply refers to the uncertainties in input, while the word "Polynomial" is used because the propagation of uncertainties is described by polynomials. If  $\zeta$  is the vector of uncertain input variables, the aim of the gPCE is to express the response function  $Y$  in the form of a polynomial  $\xi$  as follows:

$$\xi(\zeta) = \xi_0 + \xi_1 P_1(\zeta) + \xi_2 P_2(\zeta) + \dots + \xi_m P_m(\zeta) \quad (54)$$

where  $P_1, \dots, P_m$  are polynomials which form an orthogonal basis. The choice of the polynomials basis depends on the probability distribution of the input variables. In particular, for a uniform distribution, the basis of the expansion is given by the Lagrange polynomials. For the application presented in this work the coefficients of the expansion have been evaluated using a spectral projection where the computation of the required multi-dimensional integrals is based on the tensor product of one-dimensional Gaussian quadrature rules. In order to compute the quadrature points, the grid used in our work is the Clenshaw-Curtis grid (Fig. 6, right), representing a good solution for a multi-dimensional Gaussian quadrature with a small number of variables (Eldred and Burkardt, 2009).

We present here the results of several tests performed coupling the plume model with the Dakota toolkit (Adams et al., 2013) to investigate systematically the capability of the LHS and the gPCE techniques to assess the uncertainty in four response functions (plume height, solid mass flux lost and mean and variance of the mass fraction distribution at the top of the eruptive column) when the mean and the variance at the base are unknown. For all the test cases three sets of 500, 1000 and 2000 simulations have been performed for the LHS, and the results have been compared with those obtained with three tests for the gPCE and respectively 9, 36 and 81 simulations performed for the multi-dimensional quadrature. The first set of runs for the LHS, consisting of 500 simulations only, was not sufficient to provide accurate results and for this reason in the following we presents only the results obtained with 1000 and 200 simulations. In order to compare the two techniques, the cumulative distributions of the four response functions obtained with the LHS and the gPCE, have been plotted in Fig. 7 for Test Case 1 (no wind). On the  $x$ -axes we can see the range of the values obtained for the response functions: -1–3.5 for the mean of the TGSD at top of the column expressed in the  $\phi$  scale; 0.4–2.2 for the standard deviation; 10.41–10.47 km for the column height and 10%–60% for the percentage of solid mass flux lost. All the uncertainty quantification tests produced very similar results, with a small difference in the cumulative distribution observed only in the distribution of the solid mass flux lost obtained with the gPCE technique and 9 and 36 quadrature points. Similar results have been obtained for the other Test Cases (not shown here). Thus, the results highlights that for the model and the applications presented in this work gPCE represents a valid alternative to Monte Carlo simulations, with a number of runs required to produce the same accuracy reduced by

a factor 10 (81 simulations vs 1000 simulations). If more parameters were varied, the computational cost would increase for both gPCE and LHS, although the advantage of gPCE would be reduced.

585 As mentioned previously, the aim of the gPCE is to express the output of the models as polynomials and these polynomials can be used to obtain response surfaces for the output parameters as functions of the unknown input parameters through the polynomials defined by Eq. (54). In the four bottom panels of Fig. 7 the contours of the four response surfaces for the output investigated in this work have been plotted, showing the dependence on the uncertain input parameters. The mean and  
590 the standard deviation of the TGDS at the top of the eruptive column clearly reflects the corresponding values at the bottom, with a small effect of the bottom standard deviation on the mean size at the top, resulting in an increase in the average grain size with increasing values of the initial standard deviation (see the curves in the first panel bending on the left for higher values of  $\sigma$ ). Conversely, the plume height for this test case shows a non-linear dependency but at the same time a small sensitivity to the initial grain size distribution, with changes, for the specific conditions here considered,  
595 smaller than 1% of the average height. This can be explained by the fact that a large amount of air is entrained in the column during the ascent and the contribution of the solid fraction to the overall dynamics becomes small compared to that exerted by the gas. Finally, we observe that the loss of particles is mostly controlled by mean size of the TGSD.

600 In Figure 8 the same contour plots are shown for the polynomial expansion computed for Test Case 2 (top) and Test Case 3 (bottom) with 81 quadrature points. The results show again that the total grain size distribution at the base of the vent represents a reasonable approximation of that at the top of the column. For these test cases, both the column height and the solid mass lost appear to be mostly controlled by the mean size of the TGSD at the base of the column, with a small sensitivity  
605 of the height to the initial grain size distribution. We also observe that the maximum percentage of loss in the solid mass flux is about 15% for the strong plume simulations, and it is attained for larger mean sizes and smaller variance of the initial TGSD. This value is noticeably smaller than that obtained for the weak bent test case ( $\approx 40\%$ ) and for the weak test case without wind ( $\approx 60\%$ ). Despite the loss of particles, in both the cases the range of variation of the column height is quite  
610 small and, as previously mentioned, this is due to the large amount of air entrained in the volcanic column that reduces the contribution of the solid fraction to the overall dynamics. As an example to understand the relevance of the entrained air, for a simulation performed for the low-flux plume without wind and with  $\mu = 2$  and  $\sigma = 1.5$  in the  $\phi$  scale, the mass flow rate at the top of the column is  $1.2 \times 10^8$  kg/s, compared to the value at the base of  $1.5 \times 10^6$  kg/s.

#### 615 5.4 Sensitivity analysis

With the polynomial chaos expansion it is also possible to easily obtain the variance-based sensitivity indices (Saltelli et al., 2008) with no additional computational cost. In contrast with some instances, where the term sensitivity is used in a local sense to denote the computation of response

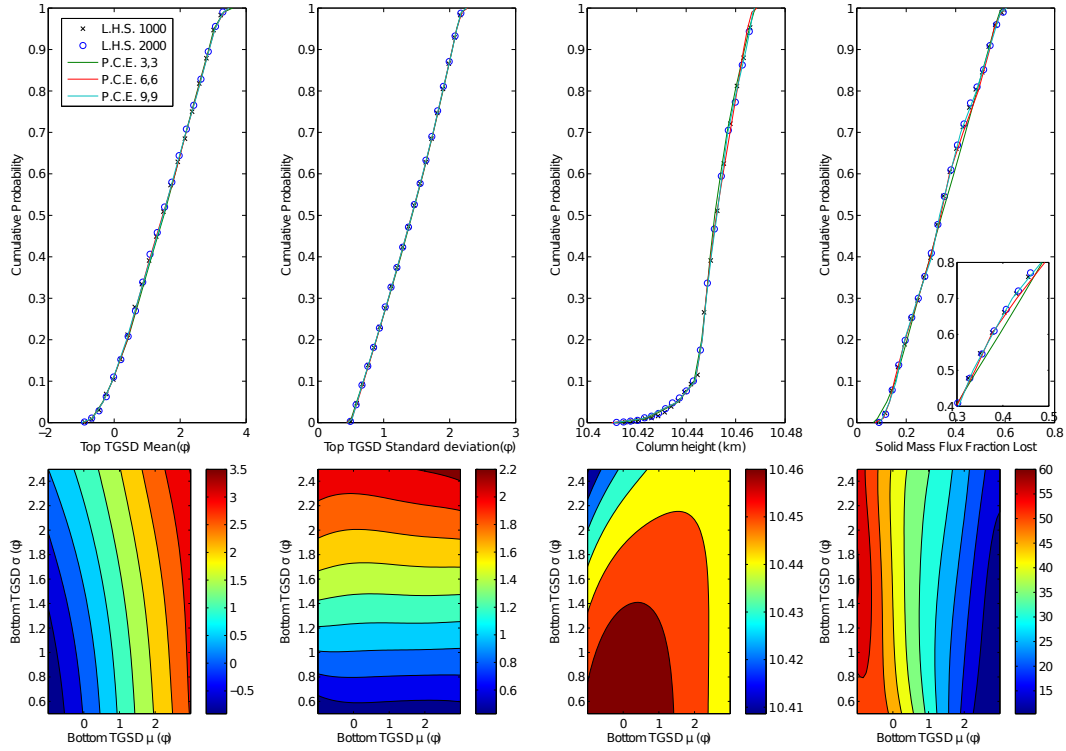


**Figure 7.** Cumulative distributions and response surfaces for test case 1 (low-flux plume without wind). In the top panels the cumulative probability for several variables describing the outcomes of the simulations (mean and variance of the grain size distribution at the top of the column, column height and cumulative fraction of solid mass lost) are plotted for the uncertainty quantification analysis carried out with the two different techniques and for different numbers of simulations. The contour plots of the response functions of the four output variables, resulting by the polynomials given by Eq. (54) and obtained with the PCE with 81 quadrature points, are plotted in the bottom panels. The variables contoured in the lower panels are the same as those on the horizontal axes in the upper panels.

derivatives at a point, here the term is used in a global sense to denote the investigation of variability in the response functions. In this context, variance-based decomposition is a global sensitivity

620 method that summarizes how the variability in model output can be apportioned to the variability in individual input variables (Adams et al., 2013). This sensitivity analysis uses two primary measures, the main effect sensitivity index  $S_i$  and the total effect index  $T_i$ . These indices are also called the Sobol indices. The main effect sensitivity index corresponds to the fraction of the uncertainty in the

625 output,  $Y$ , that can be attributed to input  $x_i$  alone. The total effects index corresponds to the fraction of the uncertainty in the output,  $Y$ , that can be attributed to input  $x_i$  and its interactions with other variables. The main effect sensitivity index compares the variance of the conditional expectation



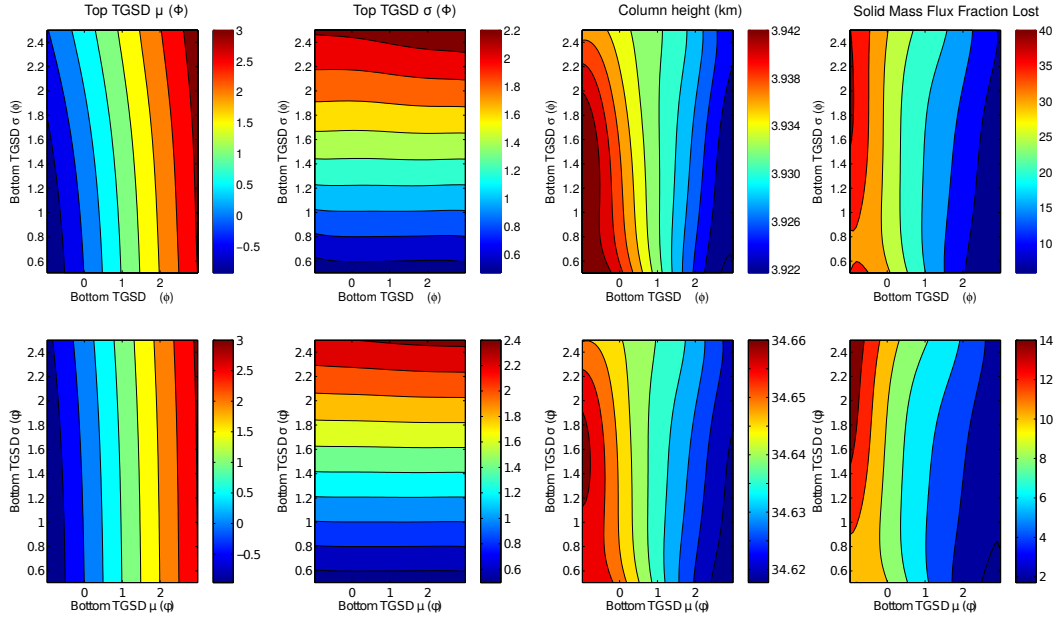


**Figure 8.** Response surfaces for Test Case 2 (low-flux plume with wind, 4 top panels) and Test Case 3 (strong plume with wind, 4 bottom panels) obtained with the PCE with 81 quadrature points. Please note that the color scale is not consistent between plots.

$Var_{x_i}[E(Y|x_i)]$  against the total variance  $Var(Y)$ . Formulas for the indices are:

$$S_i = \frac{Var_{x_i}[(Y|x_i)]}{Var(Y)} \quad (55)$$

630 and

$$T_i = \frac{E(Var(Y|X_{-i}))}{Var(Y)} \quad (56)$$

where  $Y = f(x)$  and  $x_{-i} = (x_1, \dots, x_{i-1}, x_{i+1}, \dots, x_m)$ . Similarly, it is also possible to define the sensitivity indices for higher order interactions such as the two-way interaction  $S_{i,j}$ . The calculation of  $S_i$  and  $T_i$  requires the evaluation of m-dimensional integrals which are typically approximated by  
635 Monte-Carlo sampling. However, in stochastic expansion methods, it is possible to approximate the sensitivity indices as analytic functions of the coefficients in the stochastic expansion.

The results of the sensitivity analysis for the four outputs and the three test cases investigated are presented in the bar plot of Figure 9. For each of the four groups (one for each of the different output functions) the three bars represent the main sensitivity indices for the three test cases (test  
640 1 on the left, test 2 in the middle and test 3 on the right) while the different colors are for the sensitivity indices with respect to different variables (blue is for the mean of the initial TGSD, green for the standard variation of the initial TGSD and brown for the 2nd order coupled interaction). Again, the sensitivity analysis confirms that the mean and the standard deviation of the grain size distributions at the top of the eruptive column are controlled primarily by the respective parameters

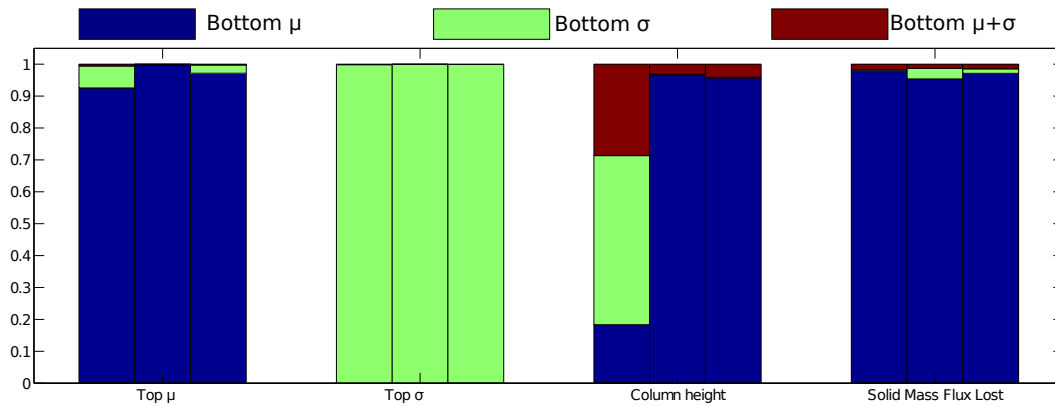


**Figure 9.** Sobol main sensitivity indices. For each of the four output parameters the three bars are for the different test cases: Test Case 1 on the left, Test Case 2 in the middle and Test Case 3 on the right. For each test case the different colors of the bars are for the different sensitivity indices: **blue for first order sensitivity index with respect to the bottom TGSD mean, green for the first order sensitivity index with respect to the bottom TGSD standard deviation and brown for the second order combined sensitivity index.**

645 of at base of the column. The mean of the TGSD also controls the percentage of solid mass flux lost during the rise of the column and the plume height for the two test cases with wind, while for the weak test case without wind the dispersion of the distribution and second-order interaction also play a major role in controlling plume height variability. However, as already observed with the uncertainty quantification analysis, we remark that the variability in the plume height, when the mean and the standard deviation of the TGSD vary in the investigated ranges, is extremely small for all the test cases (less than 1% with respect to the average values) and thus the investigation of how the variability in model output can be apportioned to the variability in individual input variables is less relevant for the plume height than for the other output parameters.

## 6 Conclusions

655 In this work we have presented an extension, based on the method of moments, of the Eulerian steady-state volcanic plume model presented in Barsotti et al. (2008) (derived from Morton (1959); Ernst et al. (1996); Bursik (2001)). Two different formulations, one based on a continuous distribution of the number of particles as a function of the size and a second based on the continuous distribution of the mass fraction, have been presented. The tracking of the moments of mass distribution, defined as a function of the Krumbein phi scale, has the advantage that with the first three moments only we are able to recover the mean and the standard deviation of the total grain size distribution. The results of a comparison between the two formulations based on the method of moments and the classical formulation based on the discretization of the mass distribution in bins show

that the different approaches produce the same results, with an advantage of the method of moments in terms of computational costs. Furthermore, a formulation based on continuous description of particle size, is better suited to properly describe complex inter-particle processes such as particle aggregation and fragmentation that are likely to play an important role in the plume evolution. In particular, the method of moments has already been successfully applied to model aggregation and breakage processes in particulate systems (Marchisio et al., 2003).

An uncertainty quantification analysis has also been applied to the formulation based on the moments of the mass distribution. The results show, for the range of conditions here investigated and neglecting likely relevant interparticle processes such as particle aggregation and comminution, a small change of the mean and variance of the particle mass distribution along the column, indicating that the total grain size distribution at the base of the vent represents a reasonable approximation of that at the top of the column. Furthermore, based on the plume model assumptions and outcomes, we observe a small sensitivity of the plume height to the initial grain size distribution, with variations of the order of tens of meters for a plume rising to several kilometers.

For the application presented in this work, involving only two parameters, the comparison between the latin hypercube sampling technique and the generalized polynomial chaos expansion method shows that the latter only requires 81 simulations to produce the same results, in terms of cumulative probability distributions of several output, obtained with 1000 simulations and the LHS. In fact, the full uncertainty quantification analysis performed on a High Performance Computing 48 multi core Shared Memory system (HPC-SM) at Istituto Nazionale di Geofisica e Vulcanologia (INGV), section of Pisa, Italy, required less than 2 seconds for the gPCE method with 81 quadrature points. These results make the new numerical code presented here, coupled with the uncertainty technique investigated, well-suited for real time hazard assessment.

## 7 Code availability

The source code with the input files for some simulation presented in this work are available for download on the Volcano Modelling and Simulation gateway (<http://vmsg.pi.ingv.it/>) and on the site for collaborative volcano research and risk mitigation Vhub (<https://vhub.org/>).

*Acknowledgements.* The authors are grateful to Samantha Engwell for the helpful discussion and suggestions on the application of the model, and to L.Mastin, Y.Suzuki and M.Wodhouse for their thorough reviews of the manuscript. This work has been partially supported by the project MEDiterranean SUPersite Volcanoes (MED-SUV) FP7 ENV.2012.6.4-2 Grant agreement no. 308665 (European Community).

695 **References**

- Adams, B.M., Bauman, L.E., Bohnhoff, W.J., Dalbey, K.R., Ebeida, M.S., Eddy, J.P., Eldred, M.S., Hough, P.D., Hu, K.T., Jakeman, J.D., Swiler, L.P., and Vigil, D.M.: DAKOTA, A Multilevel Parallel Object-Oriented Framework for Design Optimization, Parameter Estimation, Uncertainty Quantification, and Sensitivity Analysis: Version 5.4 User's Manual, Sandia Technical Report SAND2010-2183, December 2009.  
700 Updated April 2013.
- Barsotti, S., Neri, A., and Scire, J.: The VOL-CALPUFF model for atmospheric ash dispersal: 1. Approach and physical formulation, *Journal of Geophysical Research*, 113, [www.agu.org/pubs/crossref/2008/2006JB004623.shtml](http://www.agu.org/pubs/crossref/2008/2006JB004623.shtml), 2008.
- Bonadonna, C. and Phillips, J.: Sedimentation from strong volcanic plumes, *Journal of Geophysical Research*,  
705 108, 2340, 2003.
- Briggs, G. A.: Plume rise predictions, in: *Lectures on Air Pollution and Environmental Impact Analyses*, edited by Hangen, D. A., pp. 59–111, American Meteorological Society, Boston, MA, 1975.
- Bursik, M., Sparks, R., Gilbert, J., and Carey, S.: Sedimentation of tephra by volcanic plumes: I. Theory and its comparison with a study of the Fogo A plinian deposit, Sao Miguel (Azores), *Bulletin of Volcanology*,  
710 Springer, 54, 329–344, 1992.
- Bursik, M.: Effect of wind on the rise height of volcanic plumes, *Geophys. Res. Lett.*, 18, 3621–3624, 2001.
- Carey, S. and Sparks, R. S. J.: Quantitative models of the fallout and dispersal of tephra from volcanic eruption columns, *Bulletin of Volcanology*, 48, 109–125, 1986.
- Carneiro, J. N. E.: Development of a Presumed Function Method of Moments with Application to Polydisperse  
715 Sprays, Ph.D. Thesis, Technische Universität München, 2011.
- Champion, K., Cole, A., and Kantor, A. Standard and reference atmospheres *Handbook of Geophysics and the Space Environment*, Air Force Geophysics Laboratory, 14, 1985.
- Costa, A., Folch, A., and Macedonio, G.: A model for wet aggregation of ash particles in volcanic plumes and clouds: 1. Theoretical formulation, *Journal of Geophysical Research: Solid Earth*, 115, 1978–2012, 2010.
- 720 Dartevelle, S.: Numerical modeling of geophysical granular flows: 1. A comprehensive approach to granular rheologies and geophysical multiphase flows, *Geochemistry Geophysics Geosystems*, 5, 2004.
- de' Michieli Vitturi, M., Clarke, A., Neri, A., and Voight, B.: Transient effects of magma ascent dynamics along a geometrically variable dome-feeding conduit, *Earth and Planetary Science Letters*, 2010, 541–553, 295.
- Dufek, J., and Bergantz, G.: Suspended load and bed-load transport of particle-laden gravity currents: the role  
725 of particle–bed interaction, *Theoretical and Computational Fluid Dynamics*, 21, 119–145, 2007.
- Eldred, M. and Burkardt, J.: Comparison of non-intrusive polynomial chaos and stochastic collocation methods for uncertainty quantification, *AIAA paper*, 976, 1–20, 2009.
- Ernst, G. G., Sparks, R. S. J., Carey, S. N., and Bursik, M. I.: Sedimentation from turbulent jets and plumes, *Journal of Geophysical Research*, 101, 5575–5589, <http://www.agu.org/pubs/crossref/1996/95JB01900.shtml>,  
730 1996.
- Esposti Ongaro, T., Cavazzoni, C., Erbacci, G., Neri, A. and Salvetti, M. V.: A parallel multiphase flow code for the 3D simulation of explosive volcanic eruptions, *Parallel Computing*, 33, 541–560, 2007.
- Ghanem, R. and Red-Horse, J. R.: Propagation of probabilistic uncertainty in complex physical systems using a stochastic finite element technique, *Physica D*, 133, 137–144, 1999.

- 735 Gautschi, W.: *Orthogonal polynomials: computation and approximation*, Oxford University Press, 2004.
- Glaze, L. S. and Baloga, S. M.: Sensitivity of buoyant plume heights to ambient atmospheric conditions: Implications for volcanic eruption columns, *Journal of Geophysical Research*, 101, 1529–1540, 1996.
- Golub, G. H. ND Welsch, J. H.: Calculation of Gauss quadrature rules *Mathematics of computation*, 23, 221–230, 1969.
- 740 Hazewinkel, M.: *Moment*, *Encyclopedia of Mathematics*, Springer, 2001.
- Hewett, T., Fay, J. and Hoult, D.: Laboratory experiments of smokestack plumes in a stable atmosphere, *Atmospheric Environment*, Elsevier, 5, 767–789, 1971.
- Hulburt, H. M. and Katz, S.: Some problems in particle technology: A statistical mechanical formulation, *Chemical Engineering Science*, 19, 555–574, 1964.
- 745 Llewellyn, E. W., Mader, H. M. and Wilson, S. D. R.: The constitutive equation and flow dynamics of bubbly magmas, *Geophysical Research Letters*, 29, 23-1–23-4, 2002.
- Loth, E., O'Brien, T., Syamlal, M., and Cantero, M.: Effective diameter for group motion of polydisperse particle mixtures, *Powder Technology*, 142, 209–218, <http://www.sciencedirect.com/science/article/pii/S0032591004001895>, 2004.
- 750 Marchisio, D. L. and Fox, R. O.: *Computational Models for Polydisperse Particulate and Multiphase Systems*, Cambridge University Press, 2013.
- Marchisio, D. L., Vigil, R. D., and Fox, R. O.: Quadrature method of moments for aggregation–breakage processes, *Journal of Colloid and Interface Science*, 258, 322–334, 2003.
- McGraw, R.: Correcting moment sequences for errors associated with advective transport, [http://www.ecd.bnl.gov/pubs/momentcorrection\\_mcgraw2006.pdf](http://www.ecd.bnl.gov/pubs/momentcorrection_mcgraw2006.pdf), 2006.
- 755 Morton, B.: Forced plumes, *Journal of Fluid Mechanics*, 5, 151–163, 1959.
- Neri, A., Esposti Ongaro, T., Macedonio, G., and Gidaspow, D.: Multiparticle simulation of collapsing volcanic columns and pyroclastic flow, *Journal of Geophysical Research: Solid Earth*, 108, 1978–2012, 2003.
- Pal, R.: Rheological behavior of bubble-bearing magmas, *Earth and Planetary Science Letters*, 207, 165–179, 760 2003.
- Petzold, L. R. and Ascher, U. M.: *Computer methods for ordinary differential equations and differential-algebraic equations*, vol. 61, SIAM, 1998.
- Pfeiffer, T., Costa, A., and Macedonio, G.: A model for the numerical simulation of tephra fall deposits, *Journal of Volcanology and Geothermal Research*, 140, 273 – 294, doi:10.1016/j.jvolgeores.2004.09.001, 765 <http://www.sciencedirect.com/science/article/pii/S0377027304003117>, 2005.
- Rietema, K.: *The dynamics of fine powders*, Springer, 1991.
- Saltelli, A., Ratto, M., Andres, T., Campolongo, F., Cariboni, J., Gatelli, D., Saisana, M. and Tarantola, S.: *Global sensitivity analysis: the primer*, John Wiley & Sons, 2008.
- Süli, E. and Mayers, D. F.: *An introduction to numerical analysis*, Cambridge University Press, 2003.
- 770 Textor, C., Graf, H., Herzog, M., Oberhuber, J., Rose, W. I., and Ernst, G.: Volcanic particle aggregation in explosive eruption columns. Part II: Numerical experiments, *Journal of Volcanology and Geothermal Research*, 150, 378–394, <http://www.sciencedirect.com/science/article/pii/S0377027305002994>, 2006a.
- Textor, C., Graf, H.-F., Herzog, M., Oberhuber, J. M., Rose, W. I., and Ernst, G. G.: Volcanic particle aggregation in explosive eruption columns. Part I: Parameterization of the microphysics of hydrometeors and ash, *Journal*

- 775 of Volcanology and Geothermal Research, 150, 359–377, <http://www.sciencedirect.com/science/article/pii/S0377027305002982>, 2006b.
- Valentine, G. A. and Wohletz, K. H.: Numerical Models of Plinian Eruption Columns and Pyroclastic Flows, *Journal of Geophysical Research*, 94, 1867–1887, 1989.
- Weil, J.: Plume Rise, in: *Lectures on Air Pollution Modelling*, edited by Venkatram, A. and Wyngaard, J. C.,  
780 pp. 119–166, American Meteorological Society, Boston, MA, 1988.
- Woods, A. W.: The fluid dynamics and thermodynamics of eruption columns, *Bulletin of Volcanology*, 50, 169–193, <http://www.springerlink.com/index/G4M430TG5X2H9J28.pdf>, 1988.
- Wright, S. J.: Buoyant jets in density-stratified crossflow, *Journal of Hydraulic Engineering*, 110, 643–656, 1984.